AIMS Mathematics, 10(11): 27635–27665.
DOI: 10.3934/math.20251215
Received: 17 September 2025
Revised: 30 October 2025
Accepted: 06 November 2025
Published: 26 November 2025

https://www.aimspress.com/journal/Math

Research article

Application-oriented analysis of nonlinear water waves via analytical and neural network approaches; Oceanography Advances

Hassan Almusawa[1,*], **Zain Majeed**[2] **and Adil Jhangeer**[3,4,5]

[1] Department of Mathematics, College of Sciences, Jazan University, Jazan 45142, Saudi Arabia

[2] Abdus Salam School of Mathematical Sciences, Government College University, Lahore 54600, Pakistan

[3] IT4Innovations, VSB – Technical University of Ostrava, Ostrava-Poruba, Czech Republic

[4] Center for Theoretical Physics, Khazar University, 41 Mehseti Str., Baku AZ1096, Azerbaijan

[5] Department of Computer Engineering, Biruni University, Istanbul, Turkey

* **Correspondence:** Email: haalmusawa@jazanu.edu.sa.

Abstract: The fifth-order nonlinear water wave equation was explored in this and its utility in oceanography and its continued establishment was highlighted. Lie symmetry theory was applied to the nonlinear model, and the corresponding infinitesimal generators were constructed. Using the theory of abelian algebra and a suitable process of similarity reduction, the governing equation was simplified to a nonlinear ordinary differential equation. A new extended algebraic method, the nonlinear evolutionary differential approximation method, was presented to obtain the wave profiles by formulation of very general analytical solutions. To get a more detailed idea of how the physical processes that include nonlinear water waves work, 2D and 3D plots were created for several sets of parameter values, showing how the solitons were formed with unique shapes and the combined effects of dispersion and nonlinearly. In addition, a physics-informed neural network was deployed for the analysis of wave profiles. In this context, a 3D graphical representation was depicted with 2D training graphs. Additionally, by use of traveling wave transformation, 2D plots were presented to show how the wave profiles vary when parameter changes. The results, were obtained when the physics-informed neural network, were validated with a numerical scheme and revealed that the variation of parameters is crucially important to nonlinear oceanographic theories. These results support adequate parameter choices in the modeling of wave propagation and interaction in nonlinear water waves.

Keywords: Lie analysis; neural network; activation function; loss function; optimal system
Mathematics Subject Classification: 35B06, 34C14, 35Q90, 65L05

1. Introduction

The significance of nonlinear evolution equations (NLEEs) [1] has been considered outstanding in applied mathematics and nonlinear sciences [2] in general because of their capacity to represent a variety of physical phenomena. They have been commonly used to mimic complicated problems that appear in the fields of plasma physics, fluid dynamics, and many other areas of engineering. The numerical and analytical solutions of such equations have been the subject of considerable research attention over the past few decades, as documented in various papers [3, 4]. Nonlinear partial differential equations (NLPDEs) have been devised to describe an extensive variety of processes; in general, they are known as NLEEs, and can be used to model dissipation, reaction, diffusion, dispersion, and convection. Solving these equations has been deemed important in the physical sciences since solutions found can be used to describe real-world phenomena, such as the propagation of waves at finite speeds, nonlinear vibrations, and solitary wave forms, i.e., solitons. To this end, exact solution techniques and analytical solution schemes have been established and implemented in the study of NLPDEs, such that one gives a more in-depth insight into nonlinear dynamical systems.

In NLPDEs, a range of numerical and analytical methods have been used to estimate approximate or exact solutions. The finite difference method (FDM) [5], the finite element method (FEM) [6], and the finite volume method (FVM) [7] are some of the more common because of their numerical treatment. Some analytical approximation schemes have also been formulated that include the variational iteration method [8], the Adomian decomposition method [9], and the reduced differential transform method [10]. In contrast, much effort has also been focused on the creation of exact analytical solutions of NLPDEs, including those of non-integer order. In this regard, several potent methods have been presented. These are the generalized auxiliary equation method [11], the exp-function method [12], Inverse scattering transform method for nonlinear equation [13] as well as for coupled [14], the sine-cosine method [15], and the Hirota bilinear method [16–18], which have been extensively used to obtain exact solutions of nonlinear models [19, 20].

The Lie method of symmetry classification, invented by Sophus Lie in the nineteenth century, has been considered one of the most remarkable methods of obtaining new exact and explicit solutions of nonlinear partial differential equations. This has been done over the last few decades for a wide range of physical problems arising in various disciplines [21]. This method is considered a fairly mature and effective instrument of systematic investigation of nonlinear differential equations [22]. Further studies can also focus on bifurcation, chaos studies [23], sensitivity studies, [24] and lumped solutions [25].

Significant attention has been given to the determination of wave solutions to NLEEs. An important subclass of these, nonlinear wave equations (NLWWEs), has attracted considerable research attention during the last 30 years or so. The research on NLWWEs and the development of soliton solutions have been carried out by different authors. As an example, Shen and Tian [26, 27] have used the Hirota technique to obtain exact solutions of the solitons of a generalized NLWWE. Moreover, Helal et al. [28] directly used such a scheme to compute solitons of the modified dispersive equation. Ali and Seadawy [29] applied the simple equation method to obtain solitons of a shallow-water wave equation. Tian used Lie theory [30, 31] to obtain solitons of the generalized Burgers (GB) equation. Additional results on NLEEs [32, 33] and their resolution can be found in [34, 35].

In this research, we have considered the nonlinear water wave equation [36, 37] of the form:

$$A_\tau + A_\eta + \kappa_1 A A_\eta + \kappa_2 A_{\eta\eta\eta} + \kappa_3 A_\eta A_{\eta\eta} + \kappa_4 A A_{\eta\eta\eta} + \kappa_5 A_{\eta\eta\eta\eta\eta} = 0, \tag{1.1}$$

where κ_i, $i = 1, ..., 5$ are all arbitrary constants, A shows the wave packet, τ is the temporal component, and η is the spatial component. The influence of the coefficient κ_1, which is related to the quadratic nonlinear term, has been found to steepen the front of a traveling wave. The coefficient κ_3 was associated with the formation of peaks of solitary waves, or peakons. Dissipative effects are, on the other hand, incorporated into the model by coefficient κ_2, a dispersion cubic term, and the coefficient κ_5, which is a fifth-order dispersion term; these two terms are what cause the dissipation of wave packets. Moreover, the coefficient κ_4 is related to nonlinear dispersive terms of higher order. Nonlinear steepening and dispersive spreading have also been noted to be important since they enable the existence of localized and stable solitary wave solutions in a nonlinear dispersive medium. Han et al. [38] explored the nonlinear wave interactions in a generalized (3 + 1) dimensional shallow water wave equation by the Hirota bilinear method and symbolic computation and found an extensive dynamical behavior among lump, kink, breather, and rogue waves. Moreover, Han and Zhang [39] solved the KdV Calogero Bogoyavlenskii Schiff equation based on binary Bell poly theory, having obtained its bilinear Backlund transformation, Lax pair, and conservation laws [40], and mixed solutions were constructed to describe the phenomena of nonlinear shallow water waves.

Equation (1.1) was first formulated by Olver [41], and the mathematical structure of the equation was thoroughly scrutinized. Later, the soliton solutions of Eq (1.1) were obtained by the authors of [42], who obtained (1.1) using a simple computational scheme. The soliton solutions were also obtained in [43], but this was achieved using the modified tanh-method. Precise analytical solutions to Eq (1.1) were also produced in [37] and were used to show the richness in the solutions of this equation.

The Nonlinear Evolutionary Differential Approximation Method (NEDAM) has been utilized to build solutions to the nonlinear water wave equation. The approach used has also been successfully applied to the current model and is less specific and physically less significant than other methods that were used earlier. NEDAM is a potent analysis device for generating nonlinear solutions of waves, where its applicability is broader than those methods available in the literature. Moreover, this method has had a vast application in the classification and construction of the nonlinear evolution equations of all types of analytical solutions. In this way, different classes of solutions, as well as trigonometric forms explaining the creation of bright and dark solitons, have been obtained systematically. The method has also been used to find rational solutions as well as entire solutions so that it covers a wide range of potential solutions. That is why this approach has attracted great interest as an analysis approach to nonlinear dynamical systems due to its flexibility and efficiency. The applications derived from the results of NEDAM are of particular significance in applied mathematics, mathematical physics, and at the intersection of engineering sciences. In these senses, therefore, the applicability of NEDAM in generating diverse solutions to exact and generalized queries goes far beyond theoretical considerations, with implications to natural and technological phenomena of high importance in the real world.

Neural networks [44] have proven to be very promising in the area of resolution of nonlinear dynamical systems due to the ability to identify complex, nonlinear interconnections between input and output variables [45]. Neural networks have proved especially useful to simulate and forecast the dynamics of complex nonlinear systems. The high price and simplification of the underlying system

of traditional numerical methods [46] to solve complicated nonlinear differential equations [47] were inapplicable in some cases; the ability of the neural network-based method to approximate extremely complex and nonlinear relationships between the input and output variables made it suitable for solving differential equations with complex dynamics. In short, neural networks can improve management [48] and forecasting in complex nonlinear dynamical repositories spanning various fields [49], such as engineering, biology, and applied mathematics [50]. Compared to other machine learning models, PINNs can be applied in a multitude of designs of physical systems without significant variable changes to the network design. Their generality stands out as one of the major strengths that has prompted them to be embraced in interdisciplinary studies. Their capability of dealing with complex domains, non-smooth PDEs, or problems where parallelization or efficient training would be beneficial is further improved by recent developments. Singh et al. [51] provided vital results by examining the 1D and 2D Burgers equations via PINN.

Our research is structured as follows: In Section 1.1, we deal with preliminaries. In Section 2, we present the Lie symmetry analysis. In Section 3, we discuss the construction of Eq (1.1) analysis via a neural network, along with the analysis based on the traveling wave. A conclusion is provided at the end.

Preliminaries

Algorithm of the new extended direct algebraic method

Step 1): Assume the n^{th} order PDE:

$$\mathcal{F}(A, A_\eta, A_{\eta\eta}, ..., A_\tau, A_{\tau\tau}, ...) = 0. \tag{1.2}$$

Step 2): The transformation:

$$A(\tau, \eta) = \mathcal{R}(\mathtt{X}), \qquad \mathtt{X} = \tau + \mathbb{V}\eta, \tag{1.3}$$

leads to

$$\mathcal{F}(\mathcal{R}, \mathcal{R}', \mathcal{R}'', ...) = 0. \tag{1.4}$$

Step 3) : Suppose the general solution is

$$\mathcal{R}(\mathtt{X}) = \sum_{j=0}^{m} \mathcal{K}_j \mathcal{H}^j(\mathtt{X}), \qquad K_j(0 < j \leq n), \tag{1.5}$$

where $\mathcal{H}(\mathtt{X})$ holds the following expression:

$$\mathcal{H}'(\mathtt{X}) = ln(\varrho_1)(\mathcal{P}_1 + \mathcal{P}_2\mathcal{H}(\mathtt{X}) + \mathcal{P}_3\mathcal{H}^2(\mathtt{X})), \tag{1.6}$$

where $\varrho_1 \neq 0, 1$ and $\mathcal{P}_1, \mathcal{P}_2, \mathcal{P}_3$ are the constants.

After letting $\prod = {\mathcal{P}_2}^2 - 4\mathcal{P}_1\mathcal{P}_3$, the solutions of Eq. (1.6) are represented as:

1): If $\prod < 0$ and $\mathcal{P}_3 \neq 0$, then:

$$\begin{aligned}
\mathcal{H}_1(\mathtt{X}) &= -\frac{\mathcal{P}_2}{2\mathcal{P}_3} + \frac{\sqrt{-\prod}}{2\mathcal{P}_3}\tan_{\varrho_1}(\frac{\sqrt{-\prod}}{2}\mathtt{X}),\\
\mathcal{H}_2(\mathtt{X}) &= -\frac{\mathcal{P}_2}{2\mathcal{P}_3} - \frac{\sqrt{-\prod}}{2\mathcal{P}_3}\cot_{\varrho_1}(\frac{\sqrt{-\prod}}{2}\mathtt{X}),\\
\mathcal{H}_3(\mathtt{X}) &= -\frac{\mathcal{P}_2}{2\mathcal{P}_3} + \frac{\sqrt{-\prod}}{2\mathcal{P}_3}(\tan_{\varrho_1}(\sqrt{-\prod}\mathtt{X}) \pm \sqrt{rs}\sec_{\varrho_1}(\sqrt{-\prod}\mathtt{X})),\\
\mathcal{H}_4(\mathtt{X}) &= -\frac{\mathcal{P}_2}{2\mathcal{P}_3} - \frac{\sqrt{-\prod}}{2\mathcal{P}_3}(\cot_{\varrho_1}(\sqrt{-\prod}\mathtt{X}) \pm \sqrt{rs}\csc_{\varrho_1}(\sqrt{-\prod}\mathtt{X})),\\
\mathcal{H}_5(\mathtt{X}) &= -\frac{\mathcal{P}_2}{2\mathcal{P}_3} + \frac{\sqrt{-\prod}}{4\mathcal{P}_3}(\tan_{\varrho_1}(\frac{\sqrt{-\prod}}{4}\mathtt{X}) - \cot_{\varrho_1}(\frac{\sqrt{-\prod}}{4}\mathtt{X})).
\end{aligned} \tag{1.7}$$

2): If $\prod > 0$ and $\mathcal{P}_3 \neq 0$, then:

$$\begin{aligned}
\mathcal{H}_6(\mathtt{X}) &= -\frac{\mathcal{P}_2}{2\mathcal{P}_3} - \frac{\sqrt{\prod}}{2\mathcal{P}_3}\tanh_{\varrho_1}(\frac{\sqrt{\prod}}{2}\mathtt{X}),\\
\mathcal{H}_7(\mathtt{X}) &= -\frac{\mathcal{P}_2}{2\mathcal{P}_3} - \frac{\sqrt{\prod}}{2\mathcal{P}_3}\coth_{\varrho_1}(\frac{\sqrt{\prod}}{2}\mathtt{X}),\\
\mathcal{H}_8(\mathtt{X}) &= -\frac{\mathcal{P}_2}{2\mathcal{P}_3} - \frac{\sqrt{\prod}}{2\mathcal{P}_3}(\tanh_{\varrho_1}(\sqrt{\prod}\mathtt{X}) \pm \iota\sqrt{rs}\,\mathrm{sech}_{\varrho_1}(\sqrt{\prod}\mathtt{X})),\\
\mathcal{H}_9(\mathtt{X}) &= -\frac{\mathcal{P}_2}{2\mathcal{P}_3} - \frac{\sqrt{\prod}}{2\mathcal{P}_3}(\coth_{\varrho_1}(\sqrt{\prod}\mathtt{X}) \pm \sqrt{rs}\,\mathrm{csch}_{\varrho_1}(\sqrt{\prod}\mathtt{X})),\\
\mathcal{H}_{10}(\mathtt{X}) &= -\frac{\mathcal{P}_2}{2\mathcal{P}_3} - \frac{\sqrt{\prod}}{4\mathcal{P}_3}(\tanh_{\varrho_1}(\frac{\sqrt{\prod}}{4}\mathtt{X}) + \coth_{\varrho_1}(\frac{\sqrt{\prod}}{4}\mathtt{X})).
\end{aligned} \tag{1.8}$$

3): If $\mathcal{P}_3\mathcal{P}_1 > 0$ and $\mathcal{P}_2 = 0$, then:

$$\begin{aligned}
\mathcal{H}_{11}(\mathtt{X}) &= \sqrt{\frac{\mathcal{P}_1}{\mathcal{P}_3}}\tan_{\varrho_1}(\sqrt{\mathcal{P}_3\mathcal{P}_1}\mathtt{X}),\\
\mathcal{H}_{12}(\mathtt{X}) &= -\sqrt{\frac{\mathcal{P}_1}{\mathcal{P}_3}}\cot_{\varrho_1}(\sqrt{\mathcal{P}_3\mathcal{P}_1}\mathtt{X}),\\
\mathcal{H}_{13}(\mathtt{X}) &= \sqrt{\frac{\mathcal{P}_1}{\mathcal{P}_3}}(\tan_{\varrho_1}(2\sqrt{\mathcal{P}_3\mathcal{P}_1}\mathtt{X}) \pm \sqrt{rs}\sec_{\varrho_1}(2\sqrt{\mathcal{P}_3\mathcal{P}_1}\mathtt{X})),\\
\mathcal{H}_{14}(\mathtt{X}) &= \sqrt{\frac{\mathcal{P}_1}{\mathcal{P}_3}}(-\cot_{\varrho_1}(2\sqrt{\mathcal{P}_3\mathcal{P}_1}\mathtt{X}) \pm \sqrt{rs}\csc_{\varrho_1}(2\sqrt{\mathcal{P}_3\mathcal{P}_1}\mathtt{X})),\\
\mathcal{H}_{15}(\mathtt{X}) &= \frac{1}{2}\sqrt{\frac{\mathcal{P}_1}{\mathcal{P}_3}}(\tan_{\varrho_1}(\frac{\sqrt{\mathcal{P}_3\mathcal{P}_1}}{2}\mathtt{X}) - \cot_{\varrho_1}(\frac{\sqrt{\mathcal{P}_3\mathcal{P}_1}}{2}\mathtt{X})).
\end{aligned} \tag{1.9}$$

4): If $\mathcal{P}_3\mathcal{P}_1 < 0$ and $\mathcal{P}_2 = 0$, then:

$$\begin{aligned}
\mathcal{H}_{16}(\mathtt{X}) &= -\sqrt{-\frac{\mathcal{P}_1}{\mathcal{P}_3}}\tanh_{\varrho_1}(\sqrt{-\mathcal{P}_3\mathcal{P}_1}\mathtt{X}),\\
\mathcal{H}_{17}(\mathtt{X}) &= -\sqrt{-\frac{\mathcal{P}_1}{\mathcal{P}_3}}\coth_{\varrho_1}(\sqrt{-\mathcal{P}_3\mathcal{P}_1}\mathtt{X}),\\
\mathcal{H}_{18}(\mathtt{X}) &= -\sqrt{-\frac{\mathcal{P}_1}{\mathcal{P}_3}}(\tanh_{\varrho_1}(2\sqrt{-\mathcal{P}_3\mathcal{P}_1}\mathtt{X}) \pm \iota\sqrt{rs}\,\mathrm{sech}_{\varrho_1}(2\sqrt{-\mathcal{P}_3\mathcal{P}_1}\mathtt{X})),\\
\mathcal{H}_{19}(\mathtt{X}) &= -\sqrt{-\frac{\mathcal{P}_1}{\mathcal{P}_3}}(\coth_{\varrho_1}(2\sqrt{-\mathcal{P}_3\mathcal{P}_1}\mathtt{X}) \pm \sqrt{rs}\,\mathrm{csch}_{\varrho_1}(2\sqrt{-\mathcal{P}_3\mathcal{P}_1}\mathtt{X})),\\
\mathcal{H}_{20}(\mathtt{X}) &= -\frac{1}{2}\sqrt{-\frac{\mathcal{P}_1}{\mathcal{P}_3}}(\tanh_{\varrho_1}(\frac{\sqrt{-\mathcal{P}_3\mathcal{P}_1}}{2}\mathtt{X}) + \coth_{\varrho_1}(\frac{\sqrt{-\mathcal{P}_3\mathcal{P}_1}}{2}\mathtt{X})).
\end{aligned} \tag{1.10}$$

5): If $\mathcal{P}_2 = 0$ and $\mathcal{P}_3 = \mathcal{P}_1$, then:

$$\begin{aligned}
\mathcal{H}_{21}(\mathtt{X}) &= \tan_{\varrho_1}(\mathcal{P}_1\mathtt{X}),\\
\mathcal{H}_{22}(\mathtt{X}) &= -\cot_{\varrho_1}(\mathcal{P}_1\mathtt{X}),\\
\mathcal{H}_{23}(\mathtt{X}) &= \tan_{\varrho_1}(2\mathcal{P}_1\mathtt{X}) \pm \sqrt{rs}\,\sec_{\varrho_1}(2\mathcal{P}_1\mathtt{X}),\\
\mathcal{H}_{24}(\mathtt{X}) &= -\cot_{\varrho_1}(2\mathcal{P}_1\mathtt{X}) \pm \sqrt{rs}\,\csc_{\varrho_1}(2\mathcal{P}_1\mathtt{X}),\\
\mathcal{H}_{25}(\mathtt{X}) &= \frac{1}{2}(\tan_{\varrho_1}(\frac{\mathcal{P}_1}{2}\mathtt{X}) - \cot_{\varrho_1}(\frac{\mathcal{P}_1}{2}\mathtt{X})).
\end{aligned} \tag{1.11}$$

6): If $\mathcal{P}_2 = 0$ and $\mathcal{P}_3 = -\mathcal{P}_1$, then:

$$\begin{aligned}
\mathcal{H}_{26}(\mathtt{X}) &= -\tanh_{\varrho_1}(\mathcal{P}_1\mathtt{X}),\\
\mathcal{H}_{27}(\mathtt{X}) &= -\coth_{\varrho_1}(\mathcal{P}_1\mathtt{X}),\\
\mathcal{H}_{28}(\mathtt{X}) &= -\tanh_{\varrho_1}(2\mathcal{P}_1\mathtt{X}) \pm \iota\sqrt{rs}\,\mathrm{sech}_{\varrho_1}(2\mathcal{P}_1\mathtt{X}),\\
\mathcal{H}_{29}(\mathtt{X}) &= -\coth_{\varrho_1}(2\mathcal{P}_1\mathtt{X}) \pm \sqrt{rs}\,\mathrm{csch}_{\varrho_1}(2\mathcal{P}_1\mathtt{X}),\\
\mathcal{H}_{30}(\mathtt{X}) &= -\frac{1}{2}(\tanh_{\varrho_1}(\frac{\mathcal{P}_1}{2}\mathtt{X}) + \coth_{\varrho_1}(\frac{\mathcal{P}_1}{2}\mathtt{X})).
\end{aligned} \tag{1.12}$$

7): If ${\mathcal{P}_2}^2 = 4\mathcal{P}_3\mathcal{P}_1$, then:

$$\mathcal{H}_{31}(\mathtt{X}) = \frac{-2\mathcal{P}_1(\mathcal{P}_2\mathtt{X}\ln(\varrho_1) + 2)}{{\mathcal{P}_2}^2\mathtt{X}\ln(\varrho_1)}. \tag{1.13}$$

8): If $\mathcal{P}_2 = \vartheta$, $\mathcal{P}_1 = p\vartheta (p \neq 0)$ and $\mathcal{P}_3 = 0$, then:

$$\mathcal{H}_{32}(\mathtt{X}) = \varrho_1^{\vartheta\mathtt{X}} - p. \tag{1.14}$$

9): If $\mathcal{P}_2 = \mathcal{P}_3 = 0$, then:

$$\mathcal{H}_{33}(\mathtt{X}) = \mathcal{P}_1\mathtt{X}\ln(\varrho_1). \tag{1.15}$$

10): If $\mathcal{P}_2 = \mathcal{P}_1 = 0$, then:

$$\mathcal{H}_{34}(\mathtt{X}) = \frac{-1}{\mathcal{P}_3 \mathtt{X} \ln(\varrho_1)}. \tag{1.16}$$

11): If $\mathcal{P}_1 = 0$ and $\mathcal{P}_2 \neq 0$, then:

$$\begin{aligned} \mathcal{H}_{35}(\mathtt{X}) &= -\frac{r\mathcal{P}_2}{\mathcal{P}_3(\cosh_{\varrho_1}(\mathcal{P}_2\mathtt{X}) - \sinh_{\varrho_1}(\mathcal{P}_2\mathtt{X}) + r)}, \\ \mathcal{H}_{36}(\mathtt{X}) &= -\frac{\mathcal{P}_2(\sinh_{\varrho_1}(\mathcal{P}_2\mathtt{X}) + \cosh_{\varrho_1}(\mathcal{P}_2\mathtt{X}))}{\mathcal{P}_3(\sinh_{\varrho_1}(\mathcal{P}_2\mathtt{X}) + \cosh_{\varrho_1}(\mathcal{P}_2\mathtt{X}) + s)}. \end{aligned} \tag{1.17}$$

12): If $\mathcal{P}_2 = \vartheta$, $\mathcal{P}_3 = p\vartheta (p \neq 0)$ and $\mathcal{P}_1 = 0$, then:

$$\mathcal{H}_{37}(\mathtt{X}) = \frac{r\varrho_1^{\vartheta \mathtt{X}}}{s - pr\varrho_1^{\vartheta \mathtt{X}}}. \tag{1.18}$$

Step 4) : Equate the balance number m from (1.4) by highest-order nonlinear and linear terms.
Step 5): Collect the coefficients of powers of $\mathcal{H}(\mathtt{X})$ and solve the resulting system of equations.

2. Lie analysis

In this section, we apply the Lie symmetry scheme to Eq (1.1). The algorithm is shown below in terms of the important terms associated with the methodology (the readers are encouraged to refer to [22]).

The invariance condition with vector field $\mathfrak{B}$:

$$Pr^{(5)}\mathfrak{B}(A_\tau + A_\eta + \kappa_1 AA_\eta + \kappa_2 A_{\eta\eta\eta} + \kappa_3 A_\eta A_{\eta\eta} + \kappa_4 A\mathcal{A}_{\eta\eta\eta} + \kappa_5 A_{\eta\eta\eta\eta\eta} = 0.)|_{Eq.(1)=0} = 0.$$

Applying the invariance condition to Eq (1.1), we have

$$\kappa_1 A_\eta + \kappa_4 A_{\eta\eta\eta} + \Phi^\tau + \Phi^\eta + \kappa_1 A + \kappa_3 \Phi^\eta A_{\eta\eta} + \kappa_3 \Phi^{\eta\eta} A_\eta + \kappa_2 \Phi^{\eta\eta\eta} + \kappa_4 A + \kappa_5 \Phi^{\eta\eta\eta\eta\eta} = 0, \tag{2.1}$$

which leads to a two-dimensional Lie algebra:

$$\mathfrak{B}_1 = \frac{\partial}{\partial \eta}, \qquad \mathfrak{B}_2 = \frac{\partial}{\partial \tau}. \tag{2.2}$$

2.1. Optimal system

From Eq (2.2), the vector field $\mathfrak{B} = \{\mathfrak{B}_1, \mathfrak{B}_2\}$ forms an abelian algebra. Thus, the optimal system becomes:

$$\mathfrak{L}_1 = < \mathfrak{B}_1 >, \ \ \mathfrak{L}_2 = \ \ < \mathfrak{B}_1 + \mathbb{V}\mathfrak{B}_2 > . \tag{2.3}$$

Similarity reduction of Eq (1.1)

In this part, our objective is to compute the similarity variables for Eq (2.3) and then we convert the NLPDE into reduced form with the help of similarity variables and compute the analytical solution for Eq (1.1) by reduced ODE:

2.1.1. $\pounds_1 =< \mathfrak{B}_1 >$

For $\pounds_1$, we have the similarity variables:

$$A(\tau, \eta) = \mathcal{R}(\mathtt{X}), \quad \text{where } \mathtt{X} = \tau, \tag{2.4}$$

using transformation (2.4) into Eq (1.1), we get a trivial solution.

2.1.2. $\pounds_2 =< \mathfrak{B}_1 + \mathbb{V}\mathfrak{B}_2 >$

For $\pounds_2$, we have the similarity variables:

$$A(\tau, \eta) = \mathcal{R}(\mathtt{X}), \quad \text{where } \mathtt{X} = \tau + \mathbb{V}\eta. \tag{2.5}$$

Using (2.5), we get:

$$(1 + \mathbb{V})\mathcal{R}' + \kappa_1 \mathbb{V}\mathcal{R}\mathcal{R}' + \mathbb{V}^3(\kappa_2 \mathcal{R}''' + \kappa_3 \mathcal{R}'\mathcal{R}'' + \kappa_4 \mathcal{R}\mathcal{R}''') + \kappa_5 \mathbb{V}^5 \mathcal{R}''''' = 0. \tag{2.6}$$

2.2. Computation of wave packets of Eq (1.1)

In this section, the construction of the wave packets of (2.6) by NEDAM is illustrated. Eq (1.5) using $m = 2$, obtained via the balancing scheme, becomes

$$\mathcal{R}(\mathtt{X}) = \mathcal{K}_o + \mathcal{K}_1 \mathcal{H}(\mathtt{X}) + \mathcal{K}_2 \mathcal{H}^2(\mathtt{X}). \tag{2.7}$$

Suppose that $\mathcal{H}(\mathtt{X})$ is the solution of NODE:

$$\mathcal{H}'(\mathtt{X}) = ln(\varrho_1)(\mathcal{P}_1 + \mathcal{P}_2 \mathcal{H}(\mathtt{X}) + \mathcal{P}_3 \mathcal{H}^{2(\mathtt{X})}). \tag{2.8}$$

Plugging Eqs (2.7) and (2.8) into Eq (2.6), we get the system of equations. After solving the acquired system, we get the set of the solutions below:

$$\mathcal{K}_o = C_1, \quad \mathcal{K}_1 = C_2, \quad \mathcal{K}_2 = \frac{C_1 \mathcal{P}_3}{\mathcal{P}_2}, \quad \mathbb{V} = \frac{1}{\ln \varrho_1} \sqrt{\frac{C_2(-\kappa_3 - 2\kappa_5)}{60\kappa_5 \mathcal{P}_2 \mathcal{P}_3}}, \tag{2.9}$$

where C_1 and C_2 are arbitrary constants. Using Eq (2.9) in Eq (2.7), we get the following set of different wave patterns for Eq (1.1), which are represented below :

1): If $\prod < 0$ and $\mathcal{P}_3 \neq 0$, then:

$$
\begin{aligned}
A_1(\tau,\eta) =& C_1 + C_2\Big\{ -\frac{\mathcal{P}_2}{2\mathcal{P}_3} + \frac{\sqrt{-\prod}}{2\mathcal{P}_3}\tan_{\varrho_1}\big(\frac{\sqrt{-\prod}}{2}\mathtt{X}\big)\Big\} \\
&+ \frac{C_1\mathcal{P}_3}{\mathcal{P}_2}\Big(-\frac{\mathcal{P}_2}{2\mathcal{P}_3} + \frac{\sqrt{-\prod}}{2\mathcal{P}_3}\tan_{\varrho_1}\big(\frac{\sqrt{-\prod}}{2}\mathtt{X}\big)\Big)^2, \\
A_2(\tau,\eta) =& C_1 + C_2\Big\{ -\frac{\mathcal{P}_2}{2\mathcal{P}_3} - \frac{\sqrt{-\prod}}{2\mathcal{P}_3}\cot_{\varrho_1}\big(\frac{\sqrt{-\prod}}{2}\mathtt{X}\big)\Big\} \\
&+ \frac{C_1\mathcal{P}_3}{\mathcal{P}_2}\Big(-\frac{\mathcal{P}_2}{2\mathcal{P}_3} - \frac{\sqrt{-\prod}}{2\mathcal{P}_3}\cot_{\varrho_1}\big(\frac{\sqrt{-\prod}}{2}\mathtt{X}\big)\Big)^2, \\
A_3(\tau,\eta) =& C_1 + C_2\Big\{ -\frac{\mathcal{P}_2}{2\mathcal{P}_3} + \frac{\sqrt{-\prod}}{2\mathcal{P}_3}\big(\tan_{\varrho_1}\big(\sqrt{-\prod}\mathtt{X}\big) \pm \sqrt{rs}\sec_{\varrho_1}\big(\sqrt{-\prod}\mathtt{X}\big)\big)\Big\} \\
&+ \frac{C_1\mathcal{P}_3}{\mathcal{P}_2}\Big(-\frac{\mathcal{P}_2}{2\mathcal{P}_3} + \frac{\sqrt{-\prod}}{2\mathcal{P}_3}\big(\tan_{\varrho_1}\big(\sqrt{-\prod}\mathtt{X}\big) \pm \sqrt{rs}\sec_{\varrho_1}\big(\sqrt{-\prod}\mathtt{X}\big)\big)\Big)^2, \\
A_4(\tau,\eta) =& C_1 + C_2\Big\{ -\frac{\mathcal{P}_2}{2\mathcal{P}_3} - \frac{\sqrt{-\prod}}{2\mathcal{P}_3}\big(\cot_{\varrho_1}\big(\sqrt{-\prod}\mathtt{X}\big) \pm \sqrt{rs}\csc_{\varrho_1}\big(\sqrt{-\prod}\mathtt{X}\big)\big)\Big\} + \\
&\frac{C_1\mathcal{P}_3}{\mathcal{P}_2}\Big(-\frac{\mathcal{P}_2}{2\mathcal{P}_3} - \frac{\sqrt{-\prod}}{2\mathcal{P}_3}\big(\cot_{\varrho_1}\big(\sqrt{-\prod}\mathtt{X}\big) \pm \sqrt{rs}\csc_{\varrho_1}\big(\sqrt{-\prod}\mathtt{X}\big)\big)\Big)^2, \\
A_5(\tau,\eta) =& C_1 + C_2\Big\{ -\frac{\mathcal{P}_2}{2\mathcal{P}_3} + \frac{\sqrt{-\prod}}{4\mathcal{P}_3}\big(\tan_{\varrho_1}\big(\frac{\sqrt{-\prod}}{4}\mathtt{X}\big) - \cot_{\varrho_1}\big(\frac{\sqrt{-\prod}}{4}\mathtt{X}\big)\big)\Big\} + \\
&\frac{C_1\mathcal{P}_3}{\mathcal{P}_2}\Big(-\frac{\mathcal{P}_2}{2\mathcal{P}_3} + \frac{\sqrt{-\prod}}{4\mathcal{P}_3}\big(\tan_{\varrho_1}\big(\frac{\sqrt{-\prod}}{4}\mathtt{X}\big) - \cot_{\varrho_1}\big(\frac{\sqrt{-\prod}}{4}\mathtt{X}\big)\big)\Big)^2.
\end{aligned}
\tag{2.10}
$$

2): If $\prod > 0$ and $\mathcal{P}_3 \neq 0$, then:

$$
\begin{aligned}
A_6(\tau,\eta) =& C_1 - C_2\Big\{\frac{\mathcal{P}_2}{2\mathcal{P}_3} + \frac{\sqrt{\prod}}{2\mathcal{P}_3}\tanh_{\varrho_1}(\frac{\sqrt{\prod}}{2}\mathtt{X})\Big\} \\
&+ \frac{C_1\mathcal{P}_3}{\mathcal{P}_2}\Big(\frac{\mathcal{P}_2}{2\mathcal{P}_3} + \frac{\sqrt{\prod}}{2\mathcal{P}_3}\tanh_{\varrho_1}(\frac{\sqrt{\prod}}{2}\mathtt{X})\Big)^2, \\
A_7(\tau,\eta) =& C_1 - C_2\Big\{\frac{\mathcal{P}_2}{2\mathcal{P}_3} + \frac{\sqrt{\prod}}{2\mathcal{P}_3}\coth_{\varrho_1}(\frac{\sqrt{\prod}}{2}\mathtt{X})\Big\} + \frac{C_1\mathcal{P}_3}{\mathcal{P}_2}\Big(\frac{\mathcal{P}_2}{2\mathcal{P}_3} + \frac{\sqrt{\prod}}{2\mathcal{P}_3}\coth_{\varrho_1}(\frac{\sqrt{\prod}}{2}\mathtt{X})\Big)^2, \\
A_8(\tau,\eta) =& C_1 + C_2\Big\{-\frac{\mathcal{P}_2}{2\mathcal{P}_3} - \frac{\sqrt{\prod}}{2\mathcal{P}_3}(\tanh_{\varrho_1}(\sqrt{\sqrt{\prod}}\mathtt{X}) \pm \iota\sqrt{rs}\,\mathrm{sech}_{\varrho_1}(\sqrt{\sqrt{\prod}}\mathtt{X}))\Big\} \\
&+ \frac{C_1\mathcal{P}_3}{\mathcal{P}_2}\Big(-\frac{\mathcal{P}_2}{2\mathcal{P}_3} - \frac{\sqrt{\prod}}{2\mathcal{P}_3}(\tanh_{\varrho_1}(\sqrt{\sqrt{\prod}}\mathtt{X}) \pm \iota\sqrt{rs}\,\mathrm{sech}_{\varrho_1}(\sqrt{\sqrt{\prod}}\mathtt{X}))\Big)^2, \qquad (2.11) \\
A_9(\tau,\eta) =& C_1 + C_2\Big\{-\frac{\mathcal{P}_2}{2\mathcal{P}_3} - \frac{\sqrt{\prod}}{2\mathcal{P}_3}(\coth_{\varrho_1}(\sqrt{\sqrt{\prod}}\mathtt{X}) \pm \iota\sqrt{rs}\,\mathrm{csch}_{\varrho_1}(\sqrt{\sqrt{\prod}}\mathtt{X}))\Big\} \\
&+ \frac{C_1\mathcal{P}_3}{\mathcal{P}_2}\Big(-\frac{\mathcal{P}_2}{2\mathcal{P}_3} - \frac{\sqrt{\prod}}{2\mathcal{P}_3}(\coth_{\varrho_1}(\sqrt{\sqrt{\prod}}\mathtt{X}) \pm \iota\sqrt{rs}\,\mathrm{csch}_{\varrho_1}(\sqrt{\sqrt{\prod}}\mathtt{X}))\Big)^2, \\
A_{10}(\tau,\eta) =& C_1 + C_2\Big\{-\frac{\mathcal{P}_2}{2\mathcal{P}_3} - \frac{\sqrt{\prod}}{4\mathcal{P}_3}(\tanh_{\varrho_1}(\frac{\sqrt{\prod}}{4}\mathtt{X}) + \coth_{\varrho_1}(\frac{\sqrt{\prod}}{4}\mathtt{X}))\Big\} \\
&+ \frac{C_1\mathcal{P}_3}{\mathcal{P}_2}\Big(-\frac{\mathcal{P}_2}{2\mathcal{P}_3} - \frac{\sqrt{\prod}}{4\mathcal{P}_3}(\tanh_{\varrho_1}(\frac{\sqrt{\prod}}{4}\mathtt{X}) + \coth_{\varrho_1}(\frac{\sqrt{\prod}}{4}\mathtt{X}))\Big)^2.
\end{aligned}
$$

3): If $\mathcal{P}_3\mathcal{P}_1 > 0$ and $\mathcal{P}_2 = 0$, then:

$$
\begin{aligned}
A_{11}(\tau,\eta) =& C_1 + C_2\Big\{\sqrt{\frac{\mathcal{P}_1}{\mathcal{P}_3}}\tan_{\varrho_1}(\sqrt{\mathcal{P}_3\mathcal{P}_1}\mathtt{X})\Big\} + \frac{C_1\mathcal{P}_3}{\mathcal{P}_2}\Big(\sqrt{\frac{\mathcal{P}_1}{\mathcal{P}_3}}\tan_{\varrho_1}(\sqrt{\mathcal{P}_3\mathcal{P}_1}\mathtt{X})\Big)^2,\\
A_{12}(\tau,\eta) =& C_1 + C_2\Big\{-\sqrt{\frac{\mathcal{P}_1}{\mathcal{P}_3}}\cot_{\varrho_1}(\sqrt{\mathcal{P}_3\mathcal{P}_1}\mathtt{X})\Big\} + \frac{C_1\mathcal{P}_3}{\mathcal{P}_2}\Big(-\sqrt{\frac{\mathcal{P}_1}{\mathcal{P}_3}}\cot_{\varrho_1}(\sqrt{\mathcal{P}_3\mathcal{P}_1}\mathtt{X})\Big)^2,\\
A_{13}(\tau,\eta) =& C_1 + C_2\Big\{\sqrt{\frac{\mathcal{P}_1}{\mathcal{P}_3}}(\tan_{\varrho_1}(2\sqrt{\mathcal{P}_3\mathcal{P}_1}\mathtt{X}) \pm \sqrt{rs}\sec_{\varrho_1}(2\sqrt{\mathcal{P}_3\mathcal{P}_1}\mathtt{X}))\Big\}\\
&+ \frac{C_1\mathcal{P}_3}{\mathcal{P}_2}\Big(\sqrt{\frac{\mathcal{P}_1}{\mathcal{P}_3}}(\tan_{\varrho_1}(2\sqrt{\mathcal{P}_3\mathcal{P}_1}\mathtt{X}) \pm \sqrt{rs}\sec_{\varrho_1}(2\sqrt{\mathcal{P}_3\mathcal{P}_1}\mathtt{X}))\Big)^2,\\
A_{14}(\tau,\eta) =& C_1 + C_2\Big\{\sqrt{\frac{\mathcal{P}_1}{\mathcal{P}_3}}(-\cot_{\varrho_1}(2\sqrt{\mathcal{P}_3\mathcal{P}_1}\mathtt{X}) \pm \sqrt{rs}\csc_{\varrho_1}(2\sqrt{\mathcal{P}_3\mathcal{P}_1}\mathtt{X}))\Big\}\\
&+ \frac{C_1\mathcal{P}_3}{\mathcal{P}_2}\Big(\sqrt{\frac{\mathcal{P}_1}{\mathcal{P}_3}}(-\cot_{\varrho_1}(2\sqrt{\mathcal{P}_3\mathcal{P}_1}\mathtt{X}) \pm \sqrt{rs}\csc_{\varrho_1}(2\sqrt{\mathcal{P}_3\mathcal{P}_1}\mathtt{X}))\Big)^2,\\
A_{15}(\tau,\eta) =& C_1 + C_2\Big\{\frac{1}{2}\sqrt{\frac{\mathcal{P}_1}{\mathcal{P}_3}}(\tan_{\varrho_1}(\frac{\sqrt{\mathcal{P}_3\mathcal{P}_1}}{2}\mathtt{X}) - \cot_{\varrho_1}(\frac{\sqrt{\mathcal{P}_3\mathcal{P}_1}}{2}\mathtt{X}))\Big\}\\
&+ \frac{C_1\mathcal{P}_3}{\mathcal{P}_2}\Big(\frac{1}{2}\sqrt{\frac{\mathcal{P}_1}{\mathcal{P}_3}}(\tan_{\varrho_1}(\frac{\sqrt{\mathcal{P}_3\mathcal{P}_1}}{2}\mathtt{X}) - \cot_{\varrho_1}(\frac{\sqrt{\mathcal{P}_3\mathcal{P}_1}}{2}\mathtt{X}))\Big)^2.
\end{aligned}
\tag{2.12}
$$

4): If $\mathcal{P}_3\mathcal{P}_1 < 0$ and $\mathcal{P}_2 = 0$, then:

$$
\begin{aligned}
A_{16}(\tau,\eta) =& C_1 - C_2\Big\{\sqrt{-\frac{\mathcal{P}_1}{\mathcal{P}_3}}\tanh_{\varrho_1}(\sqrt{-\mathcal{P}_3\mathcal{P}_1}\mathtt{X})\Big\}\\
&+\frac{C_1\mathcal{P}_3}{\mathcal{P}_2}\Big(\sqrt{-\frac{\mathcal{P}_1}{\mathcal{P}_3}}\tanh_{\varrho_1}(\sqrt{-\mathcal{P}_3\mathcal{P}_1}\mathtt{X})\Big)^2,\\
A_{17}(\tau,\eta) =& C_1 - C_2\Big\{\sqrt{-\frac{\mathcal{P}_1}{\mathcal{P}_3}}\coth_{\varrho_1}(\sqrt{-\mathcal{P}_3\mathcal{P}_1}\mathtt{X})\Big\}\\
&+\frac{C_1\mathcal{P}_3}{\mathcal{P}_2}\Big(\sqrt{-\frac{\mathcal{P}_1}{\mathcal{P}_3}}\coth_{\varrho_1}(\sqrt{-\mathcal{P}_3\mathcal{P}_1}\mathtt{X})\Big)^2,\\
A_{18}(\tau,\eta) =& C_1 + C_2\Big\{-\sqrt{-\frac{\mathcal{P}_1}{\mathcal{P}_3}}(\tanh_{\varrho_1}(2\sqrt{-\mathcal{P}_3\mathcal{P}_1}\mathtt{X}) \pm \iota\sqrt{rs}\,\mathrm{sech}_{\varrho_1}(2\sqrt{-\mathcal{P}_3\mathcal{P}_1}\mathtt{X}))\Big\}\\
&+\frac{C_1\mathcal{P}_3}{\mathcal{P}_2}\Big(-\sqrt{-\frac{\mathcal{P}_1}{\mathcal{P}_3}}(\tanh_{\varrho_1}(2\sqrt{-\mathcal{P}_3\mathcal{P}_1}\mathtt{X}) \pm \iota\sqrt{rs}\,\mathrm{sech}_{\varrho_1}(2\sqrt{-\mathcal{P}_3\mathcal{P}_1}\mathtt{X}))\Big)^2,\\
A_{19}(\tau,\eta) =& C_1 + C_2\Big\{-\sqrt{-\frac{\mathcal{P}_1}{\mathcal{P}_3}}(\coth_{\varrho_1}(2\sqrt{-\mathcal{P}_3\mathcal{P}_1}\mathtt{X}) \pm \sqrt{rs}\,\mathrm{csch}_{\varrho_1}(2\sqrt{-\mathcal{P}_3\mathcal{P}_1}\mathtt{X}))\Big\}\\
&+\frac{C_1\mathcal{P}_3}{\mathcal{P}_2}\Big(-\sqrt{-\frac{\mathcal{P}_1}{\mathcal{P}_3}}(\coth_{\varrho_1}(2\sqrt{-\mathcal{P}_3\mathcal{P}_1}\mathtt{X}) \pm \sqrt{rs}\,\mathrm{csch}_{\varrho_1}(2\sqrt{-\mathcal{P}_3\mathcal{P}_1}\mathtt{X}))\Big)^2,\\
A_{20}(\tau,\eta) =& C_1 + C_2\Big\{-\frac{1}{2}\sqrt{-\frac{\mathcal{P}_1}{\mathcal{P}_3}}(\tanh_{\varrho_1}(\frac{\sqrt{-\mathcal{P}_3\mathcal{P}_1}}{2}\mathtt{X}) + \coth_{\varrho_1}(\frac{\sqrt{-\mathcal{P}_3\mathcal{P}_1}}{2}\mathtt{X}))\Big\}\\
&+\frac{C_1\mathcal{P}_3}{\mathcal{P}_2}\Big(-\frac{1}{2}\sqrt{-\frac{\mathcal{P}_1}{\mathcal{P}_3}}(\tanh_{\varrho_1}(\frac{\sqrt{-\mathcal{P}_3\mathcal{P}_1}}{2}\mathtt{X}) + \coth_{\varrho_1}(\frac{\sqrt{-\mathcal{P}_3\mathcal{P}_1}}{2}\mathtt{X}))\Big)^2.
\end{aligned}
\tag{2.13}
$$

5): If $\mathcal{P}_2 = 0$ and $\mathcal{P}_3 = \mathcal{P}_1$, then:

$$\begin{aligned}
A_{21}(\tau,\eta) =& C_1 + C_2\Big\{\tan_{\varrho_1}(\mathcal{P}_1\mathtt{X})\Big\} + \frac{C_1\mathcal{P}_3}{\mathcal{P}_2}\Big(\tan_{\varrho_1}(\mathcal{P}_1\mathtt{X})\Big)^2,\\
A_{22}(\tau,\eta) =& C_1 - C_2\Big\{\cot_{\varrho_1}(\mathcal{P}_1\mathtt{X})\Big\} + \frac{C_1\mathcal{P}_3}{\mathcal{P}_2}\Big(\cot_{\varrho_1}(\mathcal{P}_1\mathtt{X})\Big)^2,\\
A_{23}(\tau,\eta) =& C_1 + C_2\Big\{\tan_{\varrho_1}(2\mathcal{P}_1\mathtt{X}) \pm \sqrt{rs}\sec_{\varrho_1}(2\mathcal{P}_1\mathtt{X})\Big\}\\
&+ \frac{C_1\mathcal{P}_3}{\mathcal{P}_2}\Big(\tan_{\varrho_1}(2\mathcal{P}_1\mathtt{X}) \pm \sqrt{rs}\sec_{\varrho_1}(2\mathcal{P}_1\mathtt{X})\Big)^2,\\
A_{24}(\tau,\eta) =& C_1 + C_2\Big\{-\cot_{\varrho_1}(2\mathcal{P}_1\mathtt{X}) \pm \sqrt{rs}\csc_{\varrho_1}(2\mathcal{P}_1\mathtt{X})\Big\}\\
&+ \frac{C_1\mathcal{P}_3}{\mathcal{P}_2}\Big(-\cot_{\varrho_1}(2\mathcal{P}_1\mathtt{X}) \pm \sqrt{rs}\csc_{\varrho_1}(2\mathcal{P}_1\mathtt{X})\Big)^2,\\
A_{25}(\tau,\eta) =& C_1 + C_2\Big\{\frac{1}{2}(\tan_{\varrho_1}(\frac{\mathcal{P}_1}{2}\mathtt{X}) - \cot_{\varrho_1}(\frac{\mathcal{P}_1}{2}\mathtt{X}))\Big\}\\
&+ \frac{C_1\mathcal{P}_3}{\mathcal{P}_2}\Big(\frac{1}{2}(\tan_{\varrho_1}(\frac{\mathcal{P}_1}{2}\mathtt{X}) - \cot_{\varrho_1}(\frac{\mathcal{P}_1}{2}\mathtt{X}))\Big)^2.
\end{aligned} \tag{2.14}$$

6): If $\mathcal{P}_2 = 0$ and $\mathcal{P}_3 = -\mathcal{P}_1$, then:

$$\begin{aligned}
A_{26}(\tau,\eta) =& C_1 + C_2\Big\{-\tanh_{\varrho_1}(\mathcal{P}_1\mathtt{X})\Big\} + \frac{C_1\mathcal{P}_3}{\mathcal{P}_2}\Big(-\tanh_{\varrho_1}(\mathcal{P}_1\mathtt{X})\Big)^2,\\
A_{27}(\tau,\eta) =& C_1 + C_2\Big\{-\coth_{\varrho_1}(\mathcal{P}_1\mathtt{X})\Big\} + \frac{C_1\mathcal{P}_3}{\mathcal{P}_2}\Big(-\coth_{\varrho_1}(\mathcal{P}_1\mathtt{X})\Big)^2,\\
A_{28}(\tau,\eta) =& C_1 + C_2\Big\{-\tanh_{\varrho_1}(2\mathcal{P}_1\mathtt{X}) \pm \iota\sqrt{rs}\,\mathrm{sech}_{\varrho_1}(2\mathcal{P}_1\mathtt{X})\Big\}\\
&+ \frac{C_1\mathcal{P}_3}{\mathcal{P}_2}\Big(-\tanh_{\varrho_1}(2\mathcal{P}_1\mathtt{X}) \pm \iota\sqrt{rs}\,\mathrm{sech}_{\varrho_1}(2\mathcal{P}_1\mathtt{X})\Big)^2,\\
A_{29}(\tau,\eta) =& C_1 + C_2\Big\{-\coth_{\varrho_1}(2\mathcal{P}_1\mathtt{X}) \pm \sqrt{rs}\,\mathrm{csch}_{\varrho_1}(2\mathcal{P}_1\mathtt{X})\Big\}\\
&+ \frac{C_1\mathcal{P}_3}{\mathcal{P}_2}\Big(-\coth_{\varrho_1}(2\mathcal{P}_1\mathtt{X}) \pm \sqrt{rs}\,\mathrm{csch}_{\varrho_1}(2\mathcal{P}_1\mathtt{X})\Big)^2,\\
A_{30}(\tau,\eta) =& C_1 + C_2\Big\{-\frac{1}{2}(\tanh_{\varrho_1}(\frac{\mathcal{P}_1}{2}\mathtt{X}) + \coth_{\varrho_1}(\frac{\mathcal{P}_1}{2}\mathtt{X}))\Big\}\\
&+ \frac{C_1\mathcal{P}_3}{\mathcal{P}_2}\Big(-\frac{1}{2}(\tanh_{\varrho_1}(\frac{\mathcal{P}_1}{2}\mathtt{X}) + \coth_{\varrho_1}(\frac{\mathcal{P}_1}{2}\mathtt{X}))\Big)^2.
\end{aligned} \tag{2.15}$$

7): If ${\mathcal{P}_2}^2 = 4\mathcal{P}_3\mathcal{P}_1$, then:

$$A_{31}(\tau,\eta) = C_1 + C_2\Big\{\frac{-2\mathcal{P}_1(\mathcal{P}_2\mathtt{X}\ln(\varrho_1)+2)}{{\mathcal{P}_2}^2\mathtt{X}\ln(\varrho_1)}\Big\} + \frac{C_1\mathcal{P}_3}{\mathcal{P}_2}\Big(\frac{-2\mathcal{P}_1(\mathcal{P}_2\mathtt{X}\ln(\varrho_1)+2)}{{\mathcal{P}_2}^2\mathtt{X}\ln(\varrho_1)}\Big)^2. \tag{2.16}$$

8): If $\mathcal{P}_2 = \vartheta$, $\mathcal{P}_1 = p\vartheta (p \neq 0)$ and $\mathcal{P}_3 = 0$, then:

$$A_{32}(\tau,\eta) = C_1 + C_2\Big\{\varrho_1^{\vartheta\mathtt{X}} - p\Big\} + \frac{C_1\mathcal{P}_3}{\mathcal{P}_2}\Big(\varrho_1^{\vartheta\mathtt{X}} - p\Big)^2. \tag{2.17}$$

9): If $\mathcal{P}_2 = \mathcal{P}_3 = 0$, then:

$$A_{33}(\tau,\eta) = C_1 + C_2\Big\{\mathcal{P}_1\mathtt{X}\ln(\varrho_1)\Big\} + \frac{C_1\mathcal{P}_3}{\mathcal{P}_2}\Big(\mathcal{P}_1\mathtt{X}\ln(\varrho_1)\Big)^2. \tag{2.18}$$

10): If $\mathcal{P}_2 = \mathcal{P}_1 = 0$, then:

$$A_{34}(\tau,\eta) = C_1 + C_2\Big\{\frac{-1}{\mathcal{P}_3\mathtt{X}\ln(\varrho_1)}\Big\} + \frac{C_1\mathcal{P}_3}{\mathcal{P}_2}\Big(\frac{-1}{\mathcal{P}_3\mathtt{X}\ln(\varrho_1)}\Big)^2. \tag{2.19}$$

11): If $\mathcal{P}_1 = 0$ and $\mathcal{P}_2 \neq 0$, then:

$$\begin{aligned} A_{35}(\tau,\eta) =& C_1 + C_2\Big\{-\frac{r\mathcal{P}_2}{\mathcal{P}_3(\cosh_{\varrho_1}(\mathcal{P}_2\mathtt{X}) - \sinh_{\varrho_1}(\mathcal{P}_2\mathtt{X}) + r)}\Big\} \\ &+ \frac{C_1\mathcal{P}_3}{\mathcal{P}_2}\Big(-\frac{r\mathcal{P}_2}{\mathcal{P}_3(\cosh_{\varrho_1}(\mathcal{P}_2\mathtt{X}) - \sinh_{\varrho_1}(\mathcal{P}_2\mathtt{X}) + r)}\Big)^2, \\ A_{36}(\tau,\eta) =& C_1 + C_2\Big\{-\frac{\mathcal{P}_2(\sinh_{\varrho_1}(\mathcal{P}_2\mathtt{X}) + \cosh_{\varrho_1}(\mathcal{P}_2\mathtt{X}))}{\mathcal{P}_3(\sinh_{\varrho_1}(\mathcal{P}_2\mathtt{X}) + \cosh_{\varrho_1}(\mathcal{P}_2\mathtt{X}) + s)}\Big\} \\ &+ \frac{C_1\mathcal{P}_3}{\mathcal{P}_2}\Big(-\frac{\mathcal{P}_2(\sinh_{\varrho_1}(\mathcal{P}_2\mathtt{X}) + \cosh_{\varrho_1}(\mathcal{P}_2\mathtt{X}))}{\mathcal{P}_3(\sinh_{\varrho_1}(\mathcal{P}_2\mathtt{X}) + \cosh_{\varrho_1}(\mathcal{P}_2\mathtt{X}) + s)}\Big)^2. \end{aligned} \tag{2.20}$$

12): If $\mathcal{P}_2 = \vartheta$, $\mathcal{P}_3 = p\vartheta (p \neq 0)$ and $\mathcal{P}_1 = 0$, then:

$$A_{37}(\tau,\eta) = C_1 + C_2\Big\{\frac{r\varrho_1^{\vartheta\mathtt{X}}}{s - pr\varrho_1^{\vartheta\mathtt{X}}}\Big\} + \frac{C_1\mathcal{P}_3}{\mathcal{P}_2}\Big(\frac{r\varrho_1^{\vartheta\mathtt{X}}}{s - pr\varrho_1^{\vartheta\mathtt{X}}}\Big)^2. \tag{2.21}$$

2.2.1. Graphical representation

In this section, a graphical presentation of the results is given. The findings established are useful in explaining the importance of the NLWWE. The appropriate parameter values were chosen to display the graphical structure of the solutions obtained. The graphs obtained have demonstrated the dynamics of the equation underlying, hence gaining a better understanding of the effectiveness of nonlinear effects. The analytical results obtained are applicable in many applications, such as most notably in coastal engineering and oceanography in the prediction or control of the propagation of water waves.

The graphs below show a periodic wave appearance. The most phenomenal characteristic is the existence of very narrow, sharply pointed peaks at which the amplitude tends to infinity. In the 2D plot named Figure 2, as the timelike parameter τ varies from 0.25 to 0.75, these singularities have their position changed, and their intricate structure pattern becomes more complex. The 3D graph in Figure 1 shows these repeating walls of infinite amplitude that signify the wave instantly breaking at many different points. This phenomenon exemplifies where nonlinear steepening effects are being so dominant. These sharp and pointy crests are formed by a special solitary wave, the so-called peakon, with a discontinuity of the first derivative at the crest. It is sudden and extreme risk that has great relevance in oceanography as well as one of the main engineering design challenges in coastlines and offshore structures.

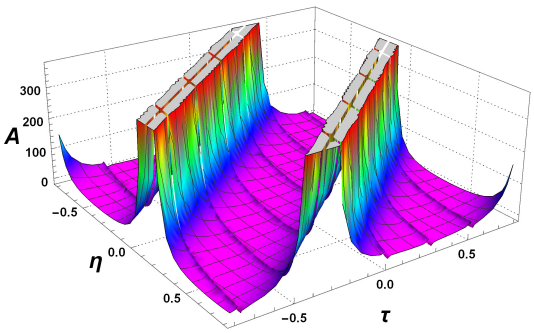

Figure 1. 3D wave profile.

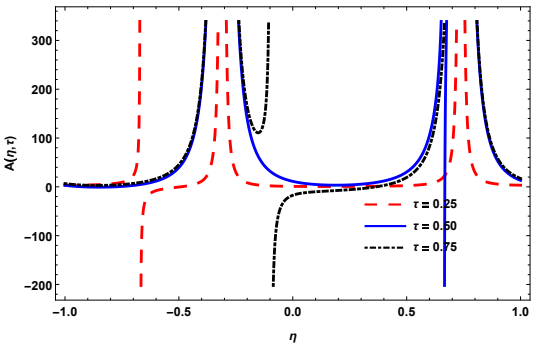

Figure 2. 2D wave profile.

Wave profile $A_1(\eta, \tau)$ for $\kappa_3 = 0.50$, $\kappa_5 = 0.75$, $\varrho_1 = e$, $\mathcal{P}_1 = 0.25$, $\mathcal{P}_2 = 0.50$, $\mathcal{P}_3 = 0.75$, $C_1 = 1$, and $C_2 = 1.5$.

Like the first pair, Figures 3 and 4 illustrate a periodic wave with sharp peaks. However, the structure is more complex. Figure 4 is a 2D representation of the problem, and it is observed that as τ increases between 3.00 and 5.00, the wave pattern evolves significantly. At $\tau = 3.00$, we see several peaks in each period. As τ increases, these peaks become overlapping and shifting. The 3D graph presented in Figure 3 illustrates a complex and repeating landscape of deep troughs and extremely high and sharp ridges. The trend is seen as an expression of a complex interplay between nonlinear and dispersive processes to suggest a very dynamic wave structure. The structure reflects the potential interplay of several unidirectional waves, in which the interaction of nonlinear modes to local amplification and modulation is achieved. The sharpness of the crests is strong, and it is in line with the dominance of the nonlinear terms that give the wave the behavior of breaking. In ocean theory, these structural features are similar to the phenomenon of energy focusing and rogue waves in the high and deep waters.

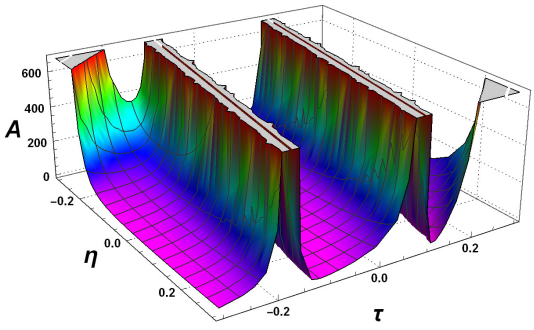

Figure 3. 3D Wave profile.

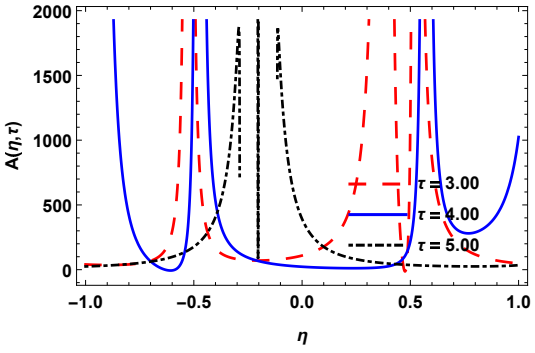

Figure 4. 2D Wave profile.

Wave Profile $A_3(\eta, \tau)$ for $\kappa_3 = 1.0$, $\kappa_5 = 1.5$, $\varrho_1 = e$, $C_1 = 1.5$ and $C_2 = 1.75$.

Figures 5 and 6 represent a different type of wave. Rather than sharp peaks, the wave has a broad profile with a noticeable dip or trough in the center ($\eta = 0$).

The general shape is smooth and well-reasoned. The 2D plot in Figure 6 indicates that when τ increases between a range of 1.50 and 3.50, a corresponding increase in amplitude is observed on the

sides of the wave together with a constant central trough.

The 3D plot in Figure 5 indicates a smooth wave profile that is intimately changing with time. This act is indication of a state where the nonlinear and dispersive effects are brought into a fine balance. The resulting structure can be taken as a dark soliton solution or a breather-type solution where the effects of dispersion essentially neutralize the effects of nonlinear steepening, thus avoiding the formation of sharp peaks or wave breakages. A balanced dynamic of this kind represents a stable propagation regime that is usually typical of self-stabilizing nonlinear systems. Considering the ocean theory and coastal engineering, this kind of solution gains useful information in predicting and controlling the dynamics of nearshore and deep-water waves, especially in the context of nonlinear modeling of ocean waves.

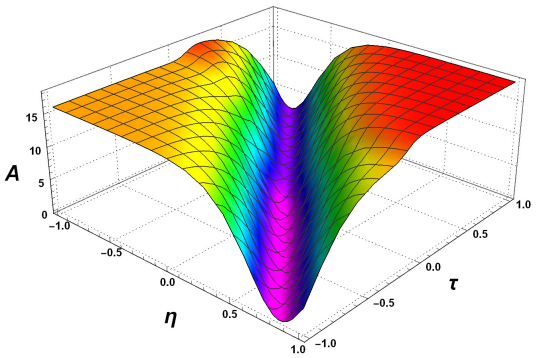

Figure 5. 3D wave profile.

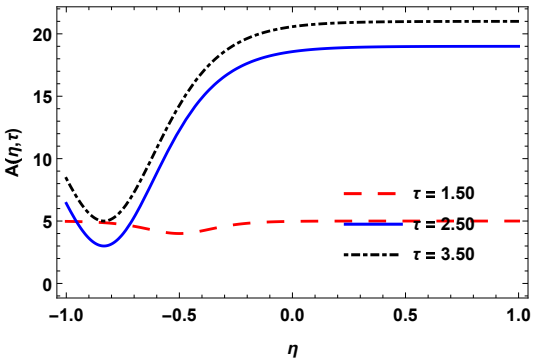

Figure 6. 2D Graphics.

Wave profile $A_6(\eta, \tau)$ for $\kappa_3 = 0.5$, $\kappa_5 = 1.5$, $\varrho_1 = e$,$C_1 = 1.5$ and $C_2 = 1.75$.

Figures 7 and 8 represent the evolution of a single localized pulse. The 2D plot in Figure 8 reveals that as the parameter of the wave, τ, increases between figure 1.00 and 3.00, the peak amplitude of the wave increases exponentially, although the width decreases. Figure 7 shows a wave pattern that is marked by spikes of progressively sharp and high values, which suggests a high concentration of energy in the waveform. This action is known to be a classic work of a solitary wave or soliton, which is a stable wave packet that does not disperse under a specific balance between the nonlinear steepening process and the dispersion spreading process. The given amplification indicates the fact that the wave is subject to an energy-focusing process, which is probably affected by the parameters governing it and making it more nonlinear than dispersive. Such findings point out the inherent stability and self reinforcing solitonic structures. In ocean theory and coastal engineering, these findings can be useful in understanding wave amplification and energy localization that are the significant factors in proper prediction of ocean waves and impact analysis of coastal areas.

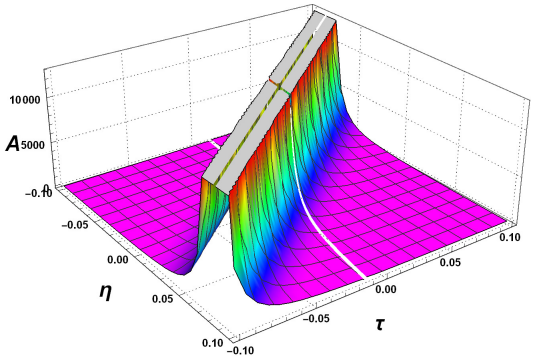

Figure 7. 3D wave profile.

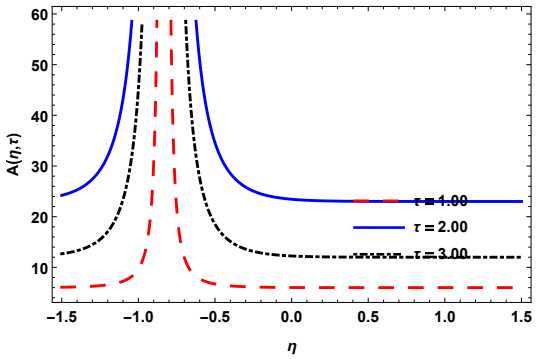

Figure 8. 2D wave profile.

Wave profile $A_7(\eta, \tau)$ for $\kappa_3 = 1.5$, $\kappa_5 = 2.5$, $\varrho_1 = e$, $C_1 = 1$ and $C_2 = 2$.

The two graphs, Figures 9 and 10, also present only a single pulse, but the behavior of the pulse differs from the ones in Figures 7 and 8. In the 2D plot in Fig. 10, the amplitude of the wave peak decreases steadily as τ changes values of 3.50 to 4.50. The wave also broadens and develops a trailing oscillatory tail. A plot of the pulse in 3D is provided in Figure 9, where the pulse is seen to get smoothed and flattened with time, showing dissipative behavior. These dispersive elements of the governing terms were discovered to expand the wave spatially, and dissipative effects cause the amplitude of the wave to reduce gradually with time. This action can be observed as a non-conservative action of energy, which is a typical feature of a real fluid system in which viscosity and internal friction are energy loss mechanisms. Dispersive dynamics of this type are useful in the study of the attenuation of energy in nonlinear media. According to the ocean theory and coastal engineering, the results could offer beneficial information in terms of modeling the wave decay, sediment transport, and energy dissipation in nearshore and deep-water systems.

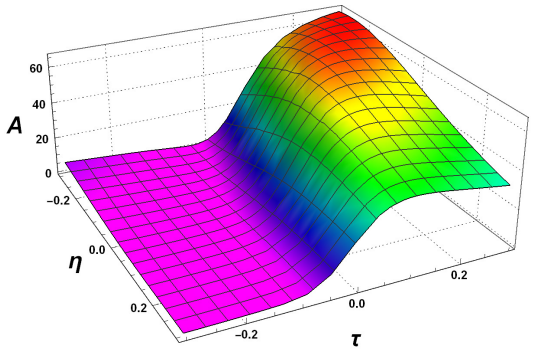

Figure 9. 3D wave profile.

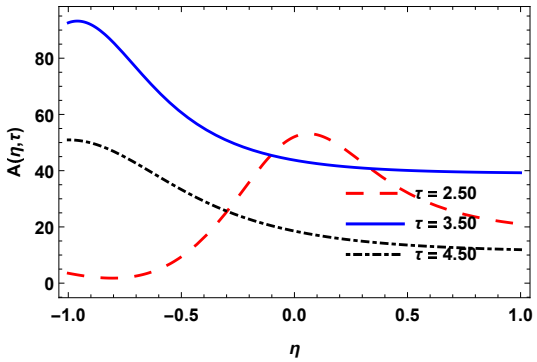

Figure 10. 2D wave profile.

Wave profile $A_8(\eta, \tau)$ for $\kappa_3 = 2$, $\kappa_5 = 5$, $\varrho_1 = e$, $C_1 = 1.5$, and $C_2 = 2.5$.

In Figures 11 and 12, wave shapes represent a very complicated interaction between waves. The 3D graph presented in Figure 11 depicts two very large and intersecting ridges where the amplitude is at extremely high levels. Figure 12 shows 2D drawings of this phenomenon at various times τ. The solution at $\tau = 3.00$ represents a periodic wave with many sharp or singular peaks, such as those of peakons presented in Figures 1–4. Compared to $\tau = 4.00$, $\tau = 5.00$ shows a very smooth wave profile with significantly lower amplitude. As τ changes to 5.00, the waves seem to flatten and spread. This

sequence illustrates a shift between a very nonlinear singular state and a smoother falling state.

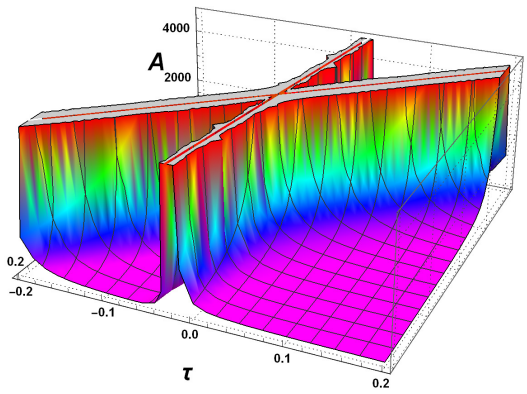

Figure 11. 3D wave profile.

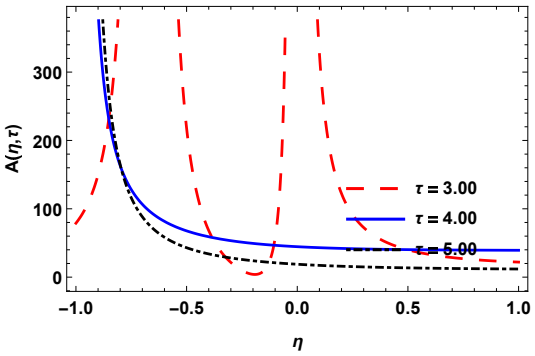

Figure 12. 2D wave profile.

Wave profile $A_9(\eta, \tau)$ for $\kappa_3 = 3.5$, $\kappa_5 = 3.75$, $\varrho_1 = e$, $C_1 = 1$, and $C_2 = 2$.

3. Analysis via the neural network

3.1. Analysis of (1.1)

The discussion of the analysis of Eq (1.1) is explained using the solution generated by PINN, as shown in Figure 13. The solution was obtained in the initial state: $u(x, 0) = x$ and the values of the boundary condition $u(0, t) = 1 = u(1, t)$ and the derivative boundary conditions $u_x(0, t) = 0 = u_x(1, t) = u_{xx}(0, t) = u_{xx}(1, t)$.

The architecture of the neural network was executed with 8 hidden layers with 128 neurons per layer, and hyperbolic tangent functions used as activation functions. The optimization was achieved with the Adam algorithm that has 6000 epochs with a learning rate of 1×10^{-3}. The coefficients were given the following values: $\kappa_1 = 1.0, \kappa_2 = 0.1, \kappa_3 = 0.05, \kappa_4 = 0.05,$ and $\kappa_5 = 0.001$.

At the initial $t = 0$ moment, there was a trough or dip in the profile value in the middle of the spatial domain. As time passed, this depression was naturally filled in, until the water surface gradually returned to a calm state. This is the process of dispersion by which localized disturbances are dispersed to occupy the domain. The time-dependent collapse of the wave is indicative of energy loss in dispersive systems, which is usually explained through dissipation mechanisms such as internal friction, turbulence, or wave spreading. In the case of our analysis, dominance of dissipative terms was the imposing of the long-term solution behavior.

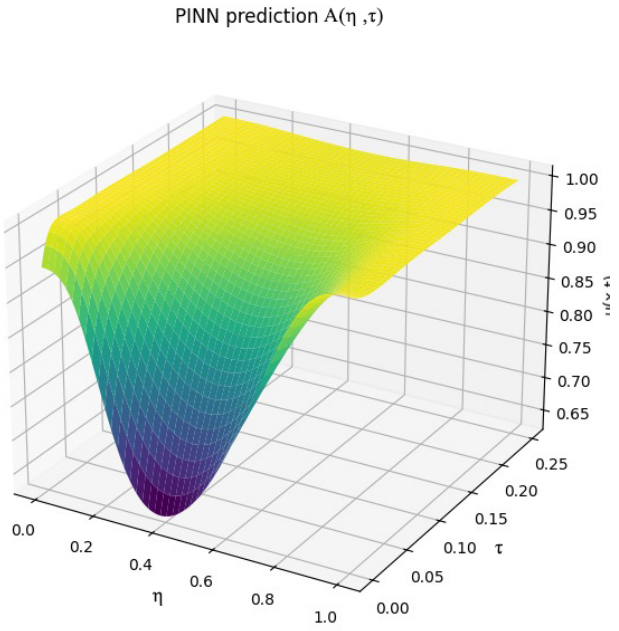

(a) 3D wave profile

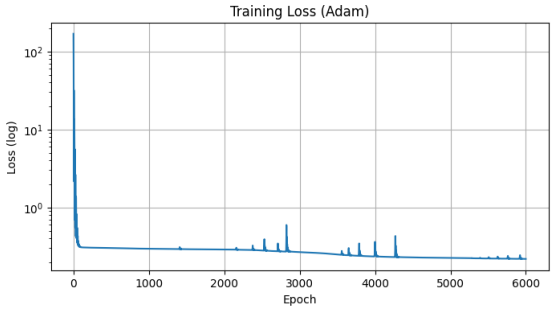

(b) Loss curve

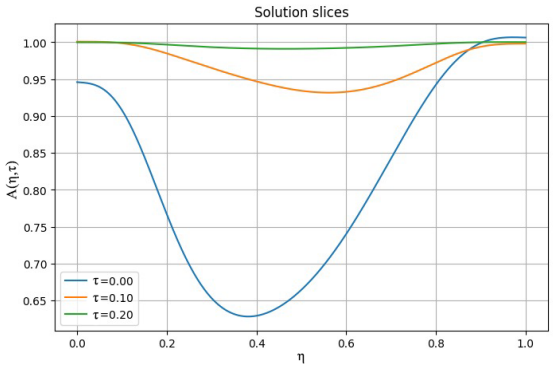

(c) 2D wave profile

Figure 13. The wave profiles for $\kappa_1 = 1.0, \kappa_2 = 0.1, \kappa_3 = 0.05, \kappa_4 = 0.05, \kappa_5 = 0.001$.

3.2. Analysis of (1.1) *via the traveling wave*

For the analysis of water wave equation (1.1), the equation:

$$(\lambda + 1)w + \kappa_1 ww' + \kappa_2 w''' + \kappa_3 w'w'' + \kappa_4 ww''' + \kappa_5 w''''' = 0, \tag{3.1}$$

by the transformation $z = \eta + \lambda\tau$. The equation is transformed into a system of ordinary equations and solved with initial conditions $y_1(0) = 0.5, y_2(0) = 1.0, y_3(0) = 0.5, y_4(0) = 0.0,$ and $y_5(0) = 0.0$. A two-layer neural network was used (128 neurons per layer), whereby the SiLU activation function was used on all the hidden units. The loss function was the mean squared error, and the learning was done using 20,000 epochs. The physics-based composite loss was defined as the total loss functional with a loss-balancing hyperparameter of 200. The Adam optimizer and an initial learning rate of 2×10^{-3} were used to perform model optimization, and a learning rate scheduler was used to guarantee stable convergence. The choice of the computational domain was $[0, 4]$.

Furthermore, to validate the neural network solution, the comparison was done using the RK method. Moreover, the RK method was stable and precise, and FCNN took a long time to train and was tuning-sensitive. FCNN was parameterized to such parameterized problems.

As κ_1 increases to 1.0 in Figure 14(a), the peak of the wave increases and its right-hand slope becomes steeper. This term has the effect of moving taller features of the wave at higher velocity; hence, the piling-up effect. By increasing the value the training, good approximations are evident.

Figure 15 shows the error heatmap.

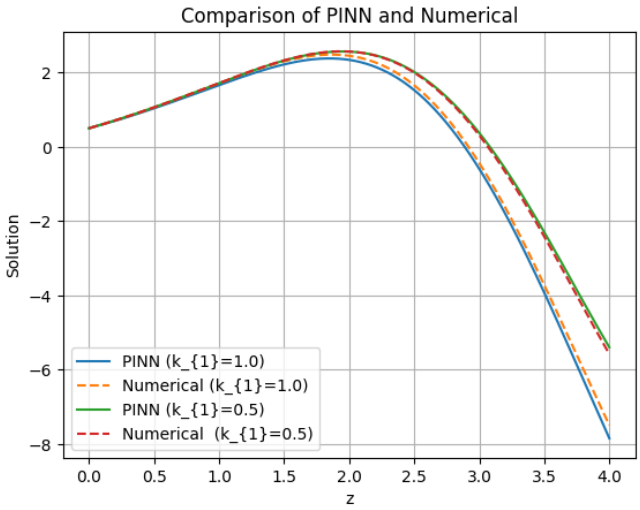

(a) The comparison of wave profiles of PINN and numerical method

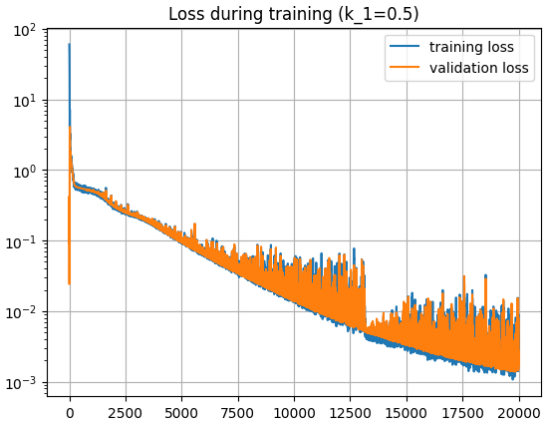

(b) Loss curve for $\kappa_1 = 0.5$

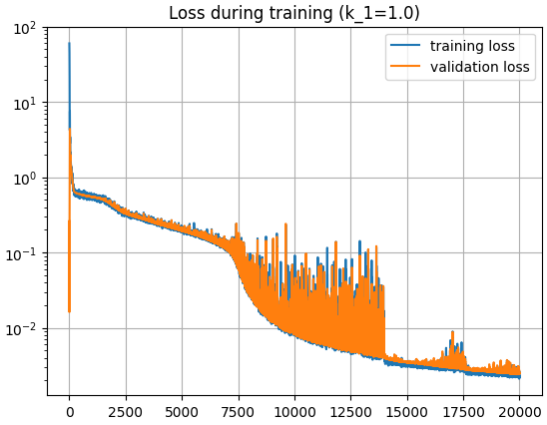

(c) Loss curve for $\kappa_1 = 1$

Figure 14. The wave profile comparison of PINN and a numerical scheme with a loss curve for different values of κ_1 with $\kappa_2 = 1.0, \kappa_3 = 1.0, \kappa_4 = 0.7, \kappa_5 = 1.0,$ and $\lambda = 2.0$.

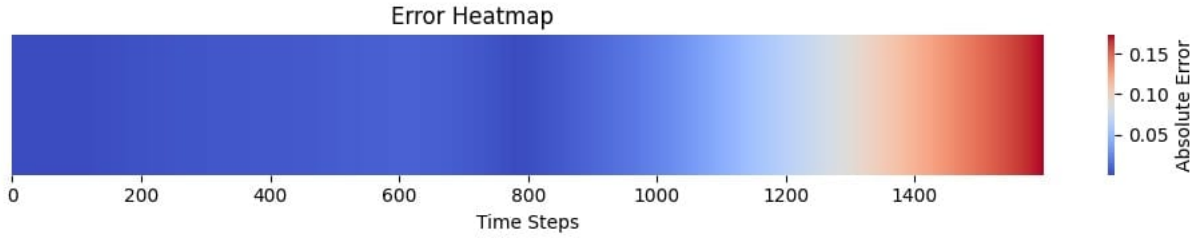

Figure 15. The heatmap error of PINN and a numerical scheme with a loss curve for different value of $\kappa_1 = 0.5\ \kappa_2 = 1.0, \kappa_3 = 1.0, \kappa_4 = 0.7, \kappa_5 = 1.0,$ and $\lambda = 2.0$.

The influence of parameter κ_2 , which governs the primary dispersive effect responsible for the spread of waves and the suppression of steepening, is illustrated in Figure 16. In Figure 16(a), an increase of κ_2 from 1.0 to 1.5 resulted in a broader and smoother wave profile. The corresponding loss curve for κ_2= 1.5 exhibited reduced complexity and enhanced smoothness, making the learning task less challenging for the PINN. As a result, the training process for κ_2=1.5 (Figure 16(c)) converged more rapidly compared to the case of κ_2= 1.0 (Figure 16 (b)), where the minimization of the losses occurred at a slower rate.

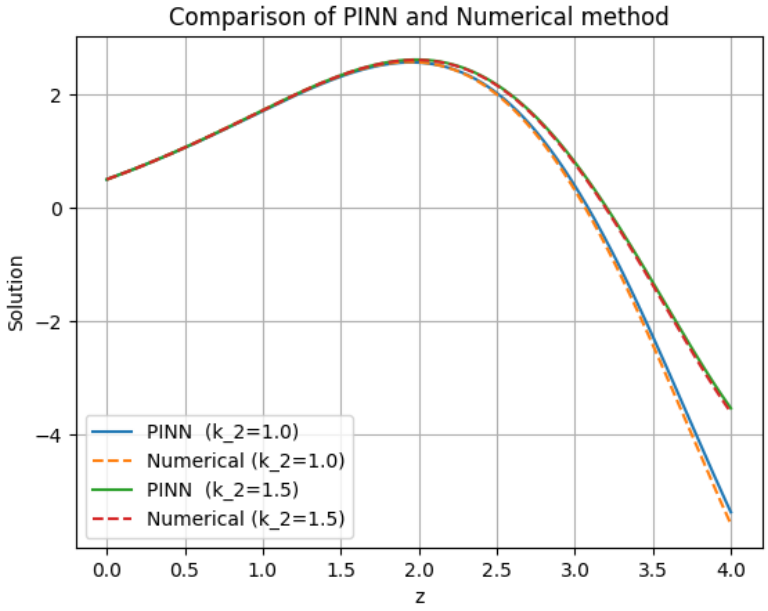

(a) The comparison of wave profiles of PINN and numerical method

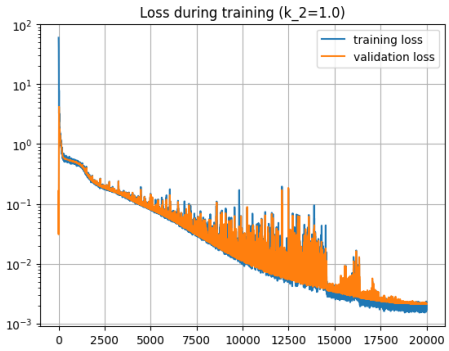

(b) Loss curve for $\kappa_2 = 1$

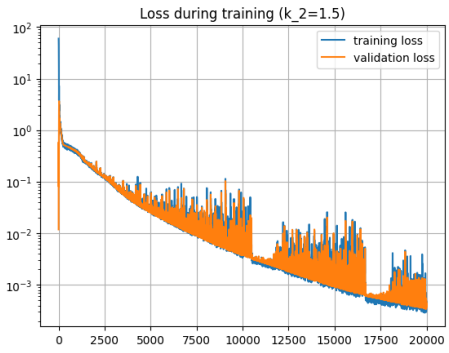

(c) Loss curve for $\kappa_2 = 1.5$

Figure 16. The wave profile comparison of PINN and a numerical scheme with a loss curve for different value of κ_2 with $\kappa_1 = 0.5, \kappa_3 = 1.0, \kappa_4 = 0.7, \kappa_5 = 1.0,$ and $\lambda = 2.0$.

Parameter κ_3 has been found to produce pointed crests considered the so-called peakons, and the attribute lies in the fact that they are sharp crests and are produced as a result of the nonlinear term. As

shown in Figure 17(a), when κ_3 increases there is a large increase in the amplitude and sharpness of the wave profile.

The solution to κ_3=1.5 with the peakon profile is much harder to teach mathematically compared to the smoother profile $\kappa_3 = 0.5$. The plots show clear evidence in the loss curves: The loss with $\kappa_3 = 1.5$ in Figure 17(c) is less convergent than that of $\kappa_3 = 0.5$ in Figure 17 (b).

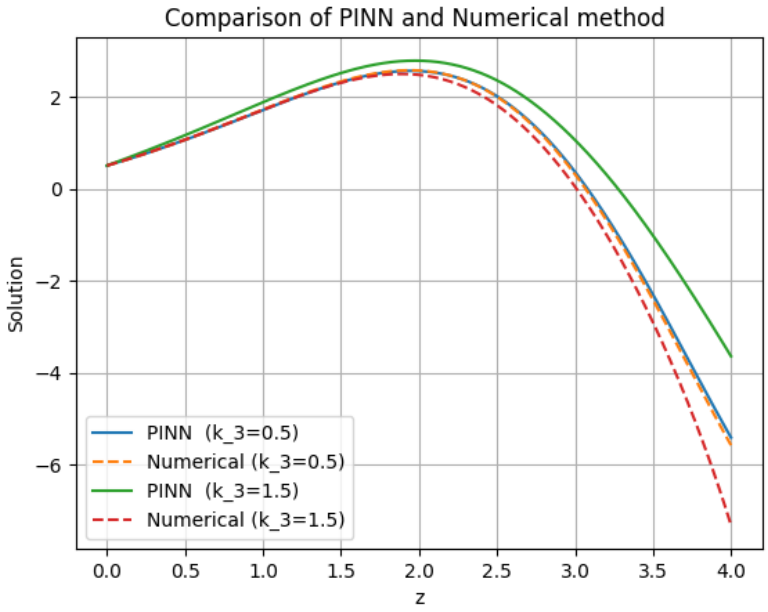

(a) The comparison of wave profiles of PINN and numerical method

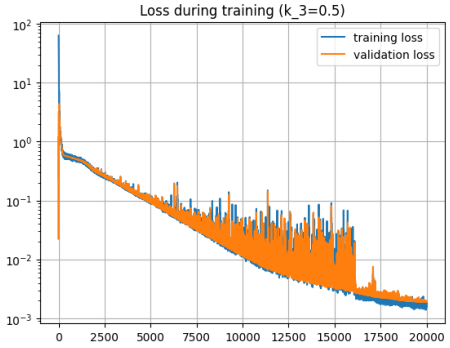

(b) Loss curve for $\kappa_3 = 0.5$

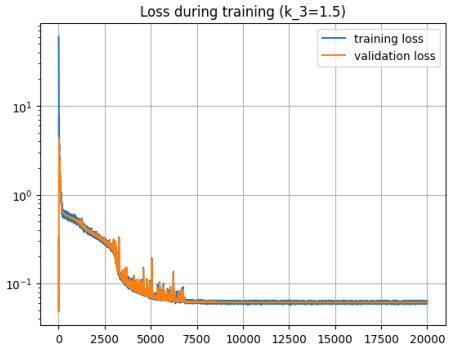

(c) Loss curve for $\kappa_3 = 1.5$

Figure 17. The wave profile comparison of PINN and a numerical scheme with a loss curve for different values of κ_3 with $\kappa_1 = 0.5, \kappa_2 = 1.0, \kappa_4 = 0.7, \kappa_5 = 1.0,$ and $\lambda = 2.0$.

Parameter κ_4 was found to be an alternative nonlinear term that helped cause the wave steepening similarly to κ_1. By increasing κ_4 to 1.5 in Figure 18(a), it was possible to obtain a taller and steeper wave profile. As in the cases of κ_1 and κ_3, the sharper solution at $\kappa = 1.5$ was also shown to be harder to approximate. Therefore, $\kappa_4 = 1.5$ in Figure 18(c) is a better convergence than $\kappa_4 = 0.7$ in Figure 18(b).

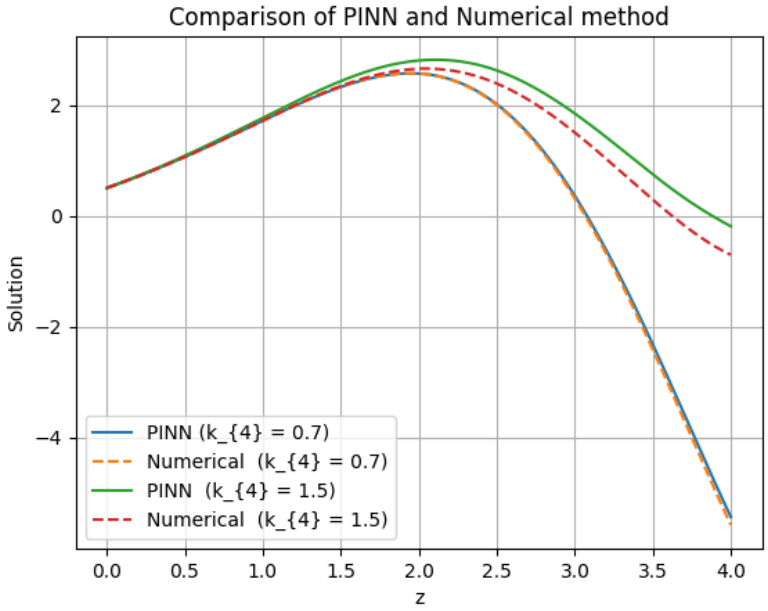

(a) The comparison of wave profiles of PINN and numerical method

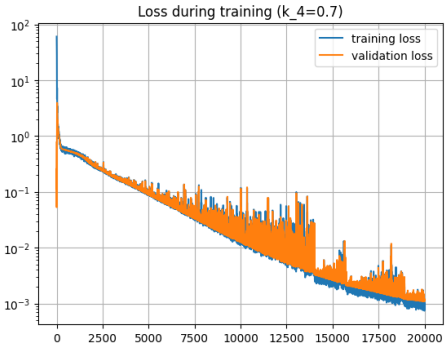

(b) Loss curve for $\kappa_4 = 0.7$

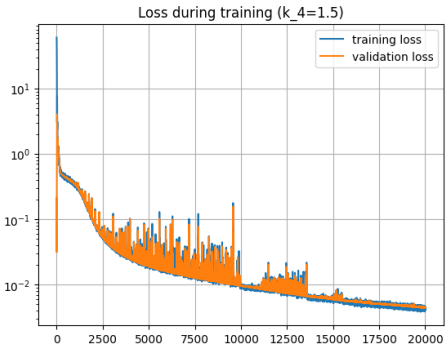

(c) Loss curve for $\kappa_4 = 1.5$

Figure 18. The wave profile comparison of PINN and a numerical scheme with a loss curve for different values of κ_4 with $\kappa_1 = 0.5, \kappa_2 = 1.0\kappa_3 = 1.0, \kappa_5 = 1.0,$ and $\lambda = 2.0$.

We found that parameter κ_5 could introduce a higher-order dispersion that helped spread the wave profile. In Figure 19(a), it was observed that the impact of an increase in κ_5 was minimal, and thus the solution was insensitive to the parameter in the given scenario for the approximation of error. Despite the insignificant difference, the solution with $\kappa_5 = 2.0$ could be seen as a bit smoother and more dispersive, which made the learning process a bit easier. This was also reinforced by the loss curves where the final loss of parameter $\kappa_5 = 2.0$ in Figure 19 (c) was lower compared to the parameter $\kappa_5 = 1.0$ in Figure 19(b).

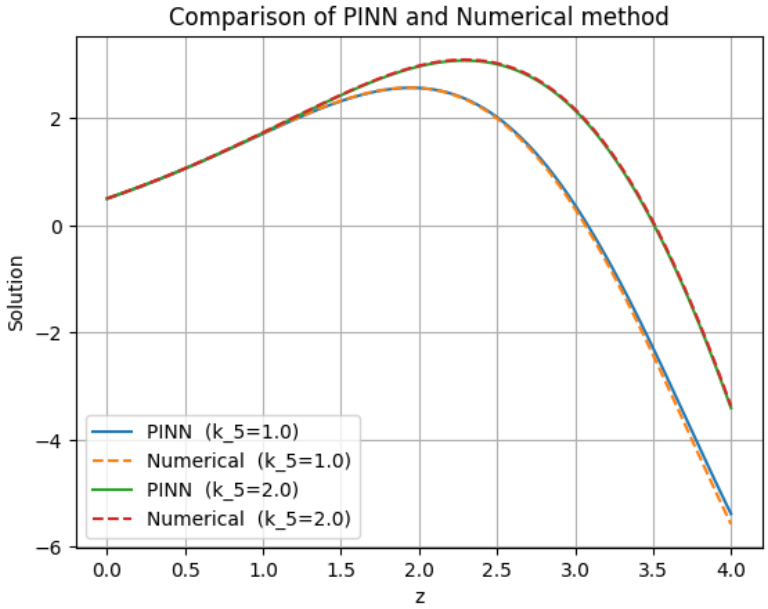

(a) The comparison of wave profiles of PINN and numerical method

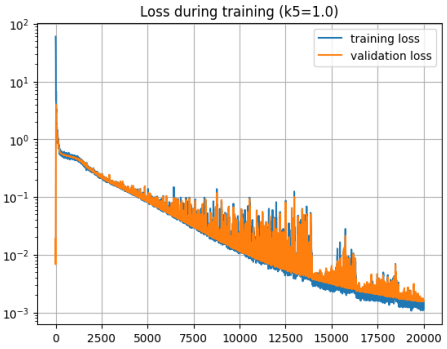

(b) Loss curve for $\kappa_5 = 1$

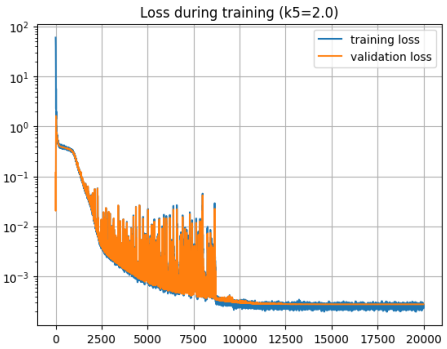

(c) Loss curve for $\kappa_5 = 2$

Figure 19. The wave profile comparison of PINN and a numerical scheme with a loss curve for different value of κ_5 with $\kappa_1 = 0.5, \kappa_2 = 1.0\kappa_3 = 1.0, \kappa_4 = 0.7,$ and $\lambda = 2.0$.

The wave solutions of two velocities, that is, $\lambda = 1$ and $\lambda = 2$, have been contrasted in Figure 20. The validation of the accuracy of the PINN was obtained because of the close agreement with the predicted solutions and the reference profiles. The near perfect coincidence of the two results indicates that the neural network framework that was used has been appropriately implemented.

The most notable finding is the change in the wave profile when the latter speed changes. When the speed increases from $l = 1.0$ to $l = 2.0$, a decrease in the peak amplitude of the wave is apparent, and the wave profile becomes less steep. This kind of response shows that the solution is sensitive to the speed of propagation.

Moreover, it is seen that by taking $\lambda = 2.0$, more numerical stiffness is introduced into the underlying ODE. The following is a result where the related optimization process becomes a challenging process to solve. This greater complexity is seen in a slightly higher final training loss compared to the case of $\lambda = 1.0$.

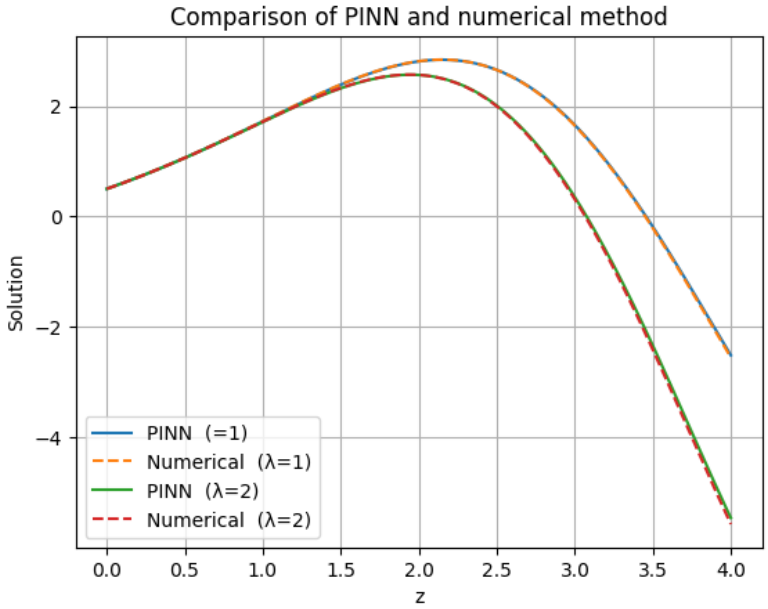

(a) The comparison of wave profiles of PINN and numerical method

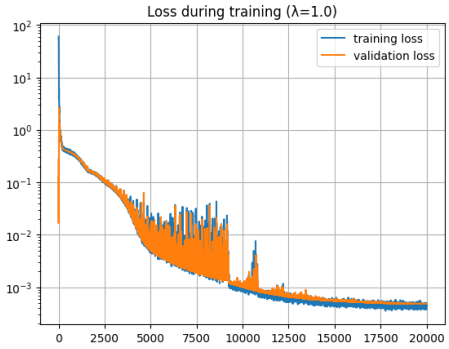

(b) Loss curve for $\lambda = 1$

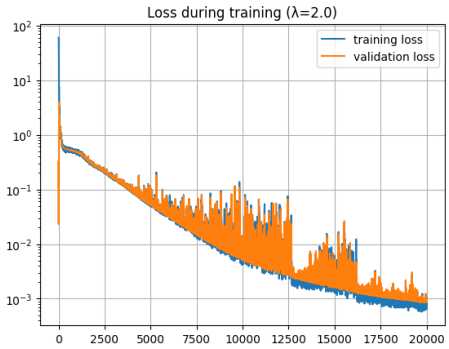

(c) Loss curve for $\lambda = 2$

Figure 20. The wave profile comparison of PINN and a numerical scheme with a loss curve for different values of λ with $\kappa_1 = 0.5, \kappa_2 = 1.0\kappa_3 = 1.0, \kappa_4 = 0.7,$ and $\kappa_5 = 1.0$.

4. Conclusions

In this analysis, we examined the uses of nonlinear water wave equations in fields of science, especially in applied mathematics. Using the Lie symmetry analysis, infinitesimal generators were found, and the obtained vector fields produced an abelian algebra. A similarity reduction scheme was used to obtain similarity variables on the basis where an optimal system was determined and that reduced the nonlinear partial differential equations to nonlinear ordinary differential equations. The NEDAM was used to obtain the solitary wave patterns, which yielded solutions in triangular and hyperbolic forms. These findings confirmed the usefulness of the method in making difficult computational tasks easier to carry out. The graphical analysis was carried out by constructing a 2D and 3D drawing that shows the travel wave profile with parameterized accuracy. It was found that different kinds of the solitons were obtained, with peaked wave solutions being produced by the high-order nonlinearities, and an impulse wave shape representing a stable wave packet, with complex wave interactions being displayed by the profiles. Additionally, there were solutions that involved a balancing act between nonlinearity and dispersion. In addition, the graphical representation of the governing equation was done with the help of PINN in which an activation function was used along with 6000 epochs. Using this pattern, time-varying dissipative effects were also observed. To explore more about the equation, we performed a traveling wave approximation and studied the effect

of changing parameters on the shape of the waves. A combination of PINN and numerical schemes were used, with the latter used to confirm neural network output through a numerical scheme. It was noted that variations in the parameters had the potential to substantially impact the training results. In particular, the nonlinear coefficients κ_3 and κ_4 had the predominant impacts on the training process. Our results of the study contribute to a computational understanding of nonlinear water waves and can be used in practice-related scenarios, such as coastal engineering and oceanography, especially when predicting and controlling wave propagation.

Future directions

Further studies to be undertaken can be guided by the expansion of this study to higher-order differential equations that occur in oceanographic modeling. The framework developed will be implemented on complex dynamical systems of interaction between wave currents, temperature diffusion, and salinity transport. Analytical and semi analytical methods will be integrated in order to make the training of the proposed method more effective and stable. The neural network structure will be tuned to nonlinear dynamics to a greater extent of accuracy. Additionally, it will be compared systematically to the traditional numerical techniques, including the finite difference and finite element methodology, concerning the convergence rate and the computational accuracy. Better generalization will be considered by hybrid strategies using data-driven and physics-based models. This will also be explored concerning the adaptability of the model to real-time ocean data assimilation. Sensitivity analysis and robustness analysis will be done for different boundaries and initial conditions. The proposed studies will focus on minimizing the cost of computation without compromising on the fidelity of large-scale simulations in the future. This trend will augment deep learning with classical numerical analysis in oceanographic studies.

Use of Generative-AI tools declaration

The authors declare they have not used Artificial Intelligence (AI) tools in the creation of this article.

Acknowledgments

This article has been produced with the financial support of the European Union under the REFRESH – Research Excellence For Region Sustainability and High-tech Industries project number CZ .10.03.01/00/22_003/0000048 via the Operational Programme Just Transition.

Conflict of interest

All authors declare that they have no competing interests.

Authors contribution

Methodology, H.A. and A.J. Software, H.A. and A.J.; Validation, H.A. and A.J.; Formal analysis, H.A., Z.M. and A.J.; Investigation, H.A., Z.M. and A.J.; Resources, H.A. and A.J.; Writing – original

draft, H.A., Z.M.and A.J.; Writing – review & editing, H.A. and A.J.; Visualization, H.A. and A.J.; Supervision, H.A. and A.J.; Project administration, H.A. and A.J.; Funding acquisition, H.A. and A.J.

A. Appendix

Here, we describe some terms involving trigonometric and hyperbolic functions used in Eq (7) to Eq (19):

$$\begin{aligned}
\sinh_{\varrho_1}(\mathtt{X}) =& \frac{r\varrho_1^{\mathtt{X}} - s\varrho_1^{-\mathtt{X}}}{2}, \qquad \cosh_{\varrho_1}(\mathtt{X}) = \frac{r\varrho_1^{\mathtt{X}} + s\varrho_1^{-\mathtt{X}}}{2},\\
\tanh_{\varrho_1}(\mathtt{X}) =& \frac{r\varrho_1^{\mathtt{X}} - s\varrho_1^{-\mathtt{X}}}{r\varrho_1^{\mathtt{X}} + s\varrho_1^{-\mathtt{X}}}, \qquad \coth_{\varrho_1}(\mathtt{X}) = \frac{r\varrho_1^{\mathtt{X}} + s\varrho_1^{-\mathtt{X}}}{r\varrho_1^{\mathtt{X}} - s\varrho_1^{-\mathtt{X}}},\\
\operatorname{csch}_{\varrho_1}(\mathtt{X}) =& \frac{2}{r\varrho_1^{\mathtt{X}} - s\varrho_1^{-\mathtt{X}}}, \qquad \operatorname{sech}_{\varrho_1}(\mathtt{X}) = \frac{2}{r\varrho_1^{\mathtt{X}} + s\varrho_1^{-\mathtt{X}}},\\
\sin_{\varrho_1}(\mathtt{X}) =& \frac{r\varrho_1^{\iota\mathtt{X}} - s\varrho_1^{-\iota\mathtt{X}}}{2\iota}, \qquad \cos_{\varrho_1}(\mathtt{X}) = \frac{r\varrho_1^{\iota\mathtt{X}} + s\varrho_1^{-\iota\mathtt{X}}}{2},\\
\tan_{\varrho_1}(\mathtt{X}) =& -\iota\frac{r\varrho_1^{\iota\mathtt{X}} - s\varrho_1^{-\iota\mathtt{X}}}{r\varrho_1^{\iota\mathtt{X}} + s\varrho_1^{-\iota\mathtt{X}}}, \qquad \cot_{\varrho_1}(\mathtt{X}) = \iota\frac{r\varrho_1^{\iota\mathtt{X}} + s\varrho_1^{-\iota\mathtt{X}}}{r\varrho_1^{\iota\mathtt{X}} - s\varrho_1^{-\iota\mathtt{X}}},\\
\csc_{\varrho_1}(\mathtt{X}) =& \frac{2\iota}{r\varrho_1^{\iota\mathtt{X}} - s\varrho_1^{-\iota\mathtt{X}}}, \qquad \operatorname{sech}_{\varrho_1}(\mathtt{X}) = \frac{2}{r\varrho_1^{\iota\mathtt{X}} + s\varrho_1^{-\iota\mathtt{X}}},
\end{aligned} \tag{A.1}$$

where r and s are constants.

References

1. M. Han, L. Zhang, Y. Wang, C. M. Khalique, The effects of the singular lines on the traveling wave solutions of modified dispersive water wave equations, *Nonlinear Anal. Real World Appl.*, **47** (2019), 236–250. https://doi.org/10.1016/j.nonrwa.2018.10.012
2. I. E. Mhlanga, C. M. Khalique, A study of a generalized Benney–Luke equation with time-dependent coefficients, *Nonlinear Dyn.*, **90** (2017), 1535–1544. https://doi.org/10.1007/s11071-017-3745-1
3. C. M. Khalique, L. D. Moleleki, A (3+1)-dimensional generalized BKP–Boussinesq equation: Lie group approach, *Results Phys.*, **13** (2019), 102239. https://doi.org/10.1016/j.rinp.2019.102239
4. Y. H. Liang, K. J. Wang, Dynamics of the new exact wave solutions to the local fractional Vakhnenko-Parkes equation, *Fractals*, (2025), 2550102. https://doi.org/10.1142/S0218348X25501026
5. L. Gavete, F. Urena, J. J. Benito, A. García, M. Urena, E. Salete, Solving second order nonlinear elliptic partial differential equations using generalized finite difference method, *J. Comput. Appl. Math.,* **318** (2018), 378–387. https://doi.org/10.1016/j.cam.2016.07.025
6. I. Christie, D. F. Griffiths, A. R. Mitchell, J. M. Sanz-Serna, Product approximation for non-linear problems in the finite element method, *IMA J. Numer. Anal.*, **1** (1981), 253–266. https://doi.org/10.1093/imanum/1.3.253

7. J. Peiró, S. Sherwin, Finite difference, finite element and finite volume methods for partial differential equations, in *Handbook of Materials Modeling: Methods* (2005), 2415–2446. https://doi.org/10.1007/978-1-4020-3286-8_127
8. M. Nadeem, F. Li, H. Ahmad, Modified Laplace variational iteration method for solving fourth-order parabolic partial differential equation with variable coefficients, *Comput. Math. Appl.*, **78** (2019), 2052–2062. https://doi.org/10.1016/j.camwa.2019.03.053
9. S. Sirisubtawee, S. Kaewta, New modified Adomian decomposition recursion schemes for solving certain nonlinear fractional two-point boundary value problems, *Int. J. Math. Math. Sci.*, (2017), 5742965. https://doi.org/10.1155/2017/5742965
10. S. Owyed, M. Abdou, A. H. Abdel-Aty, W. Alharbi, R. Nekhili, Numerical and approximate solutions for coupled time fractional nonlinear evolutions equations via reduced differential transform method, *Chaos Soliton. Fract.,* **131** (2020), 109474. https://doi.org/10.1016/j.chaos.2019.109474
11. L. Akinyemi, H. Rezazadeh, S. W. Yao, M. A. Akbar, M. M. A. Khater, A. Jhangeer, et al., Nonlinear dispersion in parabolic law medium and its optical solitons, *Results Phys.*, **26** (2021), 104411. https://doi.org/10.1016/j.rinp.2021.104411
12. J. H. He, X. H. Wu, Exp-function method for nonlinear wave equations, *Chaos Soliton. Fract.,* **30** (2008), 700–708. https://doi.org/10.1016/j.chaos.2006.03.020
13. P. F. Han, R. S. Ye, Y. Zhang, Inverse scattering transform for the coupled Lakshmanan-Porsezian-Daniel equations with non-zero boundary conditions in optical fiber communications, *Math. Comput. Simul.,* **232** (2025), 483–503. https://doi.org/10.1016/j.matcom.2025.01.008
14. P. F. Han, K. Zhu, F. Zhang, W. X. Ma, Y. Zhang, Inverse scattering transform for the fourth-order nonlinear Schrödinger equation with fully asymmetric non-zero boundary conditions, *Chin. J. Phys.*, (2025). https://doi.org/10.1016/j.cjph.2025.05.021
15. A. M. Wazwaz, A sine-cosine method for handling nonlinear wave equations, *Math. Comput. Modell.*, **40** (2004), 499–508. https://doi.org/10.1016/j.mcm.2003.12.010
16. A. M. Wazwaz, Multiple-soliton solutions for the KP equation by Hirota's bilinear method and by the tanh–coth method, *Appl. Math. Comput.,* **190** (2007), 633–640. https://doi.org/10.1016/j.amc.2007.01.056
17. K. J. Wang, Resonant multiple wave, periodic wave and interaction solutions of the new extended (3+1)-dimensional Boiti-Leon-Manna-Pempinelli equation, *Nonlinear Dyn.*, **111** (2023), 16427–16439. https://doi.org/10.1007/s11071-023-08699-x
18. K. J. Wang, The generalized (3+1)-dimensional B-type Kadomtsev-Petviashvili equation: Resonant multiple soliton, N-soliton, soliton molecules and interaction solutions, *Nonlinear Dyn.*, **112** (2024), 7309–7324. https://doi.org/10.1007/s11071-024-09356-7
19. S. Kumar, B. Kaur, S. W. Yao, M. Inc, M. S. Osman, Invariance analysis, exact solution and conservation laws of (2+1)-dimensional fractional Kadomtsev–Petviashvili system, *Symmetry*, **15** (2022), 477. https://doi.org/10.3390/sym13030477

20. M. Nadjafikhah, M. Jafari, Computation of partially invariant solutions for the Einstein-Walker manifolds' identifying equations, *Commun. Nonlinear Sci. Numer. Simul.*, **18** (2013), 3317. https://doi.org/10.1016/j.cnsns.2013.04.018

21. H. Kurkcu, M. B. Riaz, M. Imran, A. Jhangeer, Lie analysis and nonlinear propagating waves of the (3+1)-dimensional generalized Boiti-Leon-Manna-Pempinelli equation, *Alex. Eng. J.*, **80** (2023), 475–486. https://doi.org/10.1016/j.aej.2023.08.067

22. F. D. Zaman, F. M. Mahomed, F. Arif, Lie symmetry classification, optimal system and conservation laws of damped Klein-Gordon equation with power-law nonlinearity, *Math. Comput. Appl.*, **28** (2023), 96. https://doi.org/10.3390/mca28050096

23. A. Jhangeer, A. R. Ansari, M. Imran, M. B. Riaz, Beenish, Lie symmetry analysis and traveling wave patterns arise in the model of transmission lines, *AIMS Math.*, **9** (2024), 18013. https://doi.org/10.3934/math.2024878

24. A. Jhangeer, Beenish, Study of magnetic fields using dynamical patterns and sensitivity analysis, *Chaos Soliton. Fract.,* **182** (2024), 114827. https://doi.org/10.1016/j.chaos.2024.114827

25. A. Jhangeer, Beenish, Dynamics and wave analysis in longitudinal motion of elastic bars or fluids, *Ain Shams Eng. J.*, (2024), 102907. https://doi.org/10.1016/j.asej.2024.102907

26. Y. Shen, B. Tian, Bilinear auto-Bäcklund transformations and soliton solutions of a (3+1)-dimensional generalized nonlinear evolution equation for shallow water waves, *Appl. Math. Lett.*, **122** (2021), 107301. https://doi.org/10.1016/j.aml.2021.107301

27. Y. Shen, B. Tian, S. H. Liu, Solitonic fusion and fission for a (3+1)-dimensional generalized nonlinear evolution equation arising in the shallow water waves, *Phys. Lett. A*, **405** (2021), 127429. https://doi.org/10.1016/j.physleta.2021.127429

28. M. A. Helal, A. R. Seadawy, M. Zekry, Stability analysis solutions of the nonlinear modified Degasperis–Procesi water wave equation, *J. Ocean Eng. Sci.*, **2** (2017), 155–160. https://doi.org/10.1016/j.joes.2017.07.002

29. A. Ali, A. R. Seadawy, Dispersive soliton solutions for shallow water wave system and modified Benjamin–Bona–Mahony equations, *J. Ocean Eng. Sci.*, **6** (2021), 85–98. https://doi.org/10.1016/j.joes.2020.06.001

30. M. Devi, S. Yadav, R. Arora, Optimal system and invariance analysis of fourth-order nonlinear Ablowitz-Kaup-Newell-Segur water wave dynamical equation using Lie symmetry approach, *Appl. Math. Comput.*, **404** (2021), 126230. https://doi.org/10.1016/j.amc.2021.126230

31. H. Almusawa, A. Jhangeer, Beenish, Soliton solutions, Lie symmetry analysis and conservation laws of ionic waves traveling through microtubules in live cells, *Results Phys.*, **43** (2022), 106028. https://doi.org/10.1016/j.rinp.2022.106028

32. X. Hong, A. Ilyas, A. Alkireet, O. A. Ilhan, J. Manafian, M. K. M. Nasution, Multiple soliton solutions of the generalized Hirota-Satsuma-Ito equation arising in shallow water wave, *J. Geom. Phys.*, (2021), 104338. https://doi.org/10.1016/j.geomphys.2021.104338

33. U. Younas, A. R. Seadawy, M. Younis, S. T. R. Rizvi, Dispersive propagation wave structures of the Dullin-Gottwald-Holm dynamical equation in shallow water waves, *Chin. J. Phys.*, **68** (2020), 348–364. https://doi.org/10.1016/j.cjph.2020.09.021

34. F. S. Alshammari, M. F. Hoque, H. O. Rashid, Dynamical solitary interactions between lump waves and different forms of solitons for the (2+1)-dimensional shallow water wave equation, *Partial Differ. Equ. Appl. Math.*, **3** (2021), 100026. https://doi.org/10.1016/j.padiff.2021.100026

35. N. Yang, W. Xu, K. Zhang, B. Zheng, Exact solutions to the space-time fractional shallow water wave equation via complete discrimination system for polynomial method, *Results Phys.*, **20** (2021), 103728. https://doi.org/10.1016/j.rinp.2020.103728

36. K. Hosseini, M. Mirzazadeh, S. Salahshour, D. Baleanu, A. Zafar, Specific wave structures of a fifth-order nonlinear water wave equation, *J. Ocean Eng. Sci.*, **14** (2021). https://doi.org/10.1016/j.joes.2021.09.019

37. K. Hosseini, M. Inc, M. Shafiee, M. Ilie, A. Shafaroody, A. Yusuf, et al., Invariant subspaces, exact solutions and stability analysis of nonlinear water wave equations, *J. Ocean Eng. Sci.,* **5** (2020), 35–40. https://doi.org/10.1016/j.joes.2019.07.004

38. P. F. Han, K. Zhu, W. X. Ma, Novel superposition solutions for an extended (3+1)-dimensional generalized shallow water wave equation in fluid mechanics and plasma physics, *Qual. Theory Dyn. Syst.,* **24** (2025), 150. https://doi.org/10.1007/s12346-025-01310-1

39. P. F. Han, Y. Zhang, Investigation of shallow water waves near the coast or in lake environments via the KdV-Calogero-Bogoyavlenskii-Schiff equation, *Chaos Solit. Fract.,* **184** (2024), 115008. https://doi.org/10.1016/j.chaos.2024.115008

40. E. Noether, Invariante Variationsprobleme, *Nachr. König. Ges. Wiss. Gött. Math.-Phys. Kl.*, **2** (1918), 235–257. https://doi.org/10.48550/arXiv.physics/0503066

41. P. J. Olver, *Hamiltonian and Non-Hamiltonian Models for Water Waves*, Springer, (1984). https://doi.org/10.1007/3-540-12916-2_62

42. H. Lu, M. Wang, Exact soliton solutions of some nonlinear physical models, *Phys. Lett. A*, **255** (1999), 249–252. https://doi.org/10.1016/S0375-9601(03)00909-5

43. A. H. A. Ali, A. A. Soliman, New exact solutions of some nonlinear partial differential equations, *Int. J. Nonlinear Sci.*, **5** (2008), 79–88.

44. J. Ul Rahman, F. Makhdoom, A. Ali, S. Danish, Mathematical modeling and simulation of biophysics systems using neural network, *Int. J. Mod. Phys. B*, **38** (2024), 2450066. https://doi.org/10.1142/S0217979224500668

45. S. Rehman, A. Hussain, J. Ul Rahman, N. Anjum, T. Munir, Modified Laplace based variational iteration method for the mechanical vibrations and its applications, *Acta Mech. Autom.*, **16** (2022), 2. https://doi.org/10.2478/ama-2022-0012

46. J. A. Zarnan, W. M. Hameed, A. B. Kanbar, New numerical approach for solution of nonlinear differential equations, *J. Hunan Univ. Nat. Sci.*, **49** (2022), 7. https://doi.org/10.55463/issn.1674-2974.49.7.18

47. S. Kremsner, A. Steinicke, M. Szölgyenyi, A deep neural network algorithm for semilinear elliptic PDEs with applications in insurance mathematics, *Risks*, **8** (2020), 136. https://doi.org/10.3390/risks8040136

48. Y. Li, W. Han, H. Zheng, J. Huang, W. Wang, Deep learning-based safety helmet detection in engineering management based on convolutional neural networks, *Adv. Civ. Eng.*, (2020), 9703560. https://doi.org/10.1155/2020/9703560

49. A. Sahu, K. P. S. Rana, V. Kumar, An application of deep dual convolutional neural network for enhanced medical image denoising, *Med. Biol. Eng. Comput.*, **61** (2023), 991–1004. https://doi.org/10.1007/s11517-022-02731-9

50. G. Pan, P. Zhang, A. Chen, Y. Deng, Z. Zhang, H. Lu, et al., Aerobic glycolysis in colon cancer is repressed by naringin via the HIF1A pathway, *J. Zhejiang Univ. Sci. B*, **24** (2023), 221–231. https://doi.org/10.1631/jzus.B2200221

51. A. Singh, R. Jiwari, U. Saini, PINNs algorithmic framework for simulation of nonlinear Burgers' type models, *arXiv preprint* arXiv:2506.12922 (2025). https://doi.org/10.48550/arXiv.2506.12922

AIMS Press